LI-RADS Version 2018 Ancillary Features at MRI

Authors
Milena Cerny, MD
Victoria Chernyak, MD MS
Damien Olivié, MD
Jean-Sébastien Billiard, MD
Jessica Murphy-Lavallée, MD
Ania Z. Kielar, MD
Khaled M. Elsayes, MD
Laurence Bourque
Jonathan C. Hooker, BS
Claude B. Sirlin, MD
An Tang, MD, MSc

Affiliations
From the Department of Radiology, Centre Hospitalier de l'Université de Montréal, 1000 rue Saint-Denis, Montréal, QC, Canada H2X 0C2 (M.C., D.O., J.S.B., J.M.L., L.B., A.T.);
Centre de Recherche du Centre Hospitalier de l'Université de Montréal, Montréal, Quebec, Canada (M.C., A.T.); Department of Radiology, Montefiore Medical Center, Bronx, NY (V.C.); Department of Radiology, University of Ottawa, Ottawa, Ontario, Canada (A.Z.K.); Department of Diagnostic Radiology, University of Texas MD Anderson Cancer Center, Houston, Tex (K.M.E.); and Liver Imaging Group, Department of Radiology, University of California San Diego, San Diego, Calif (J.C.H., C.B.S.). Recipient of a Certificate of Merit award for an educa- tion exhibit at the 2017 RSNA Annual Meeting. Received March 4, 2018; revision requested April 10 and received May 10; accepted May 11. For this journal-based SA-CME activity, the authors A.Z.K. and C.B.S. have provided disclosures (see end of article); all other authors, the editor, and the reviewers have disclosed no relevant relationships.

Address correspondence
A.T. (e-mail: an.tang@umontreal.ca).

M.C. supported by Bourse Université de Mon-tréal and Fondation Centre Hospitalier de l'Université de Montréal. A.T. supported by the Fonds de Recherche du Québec en Santé and Fondation de l'Association des Radiologistes du Québec (Clinical Research Scholarship–Junior 2 Salary Award 34939).

Disclosures of Conflicts of Interest.—A.Z.K. *Activities related to the present article:* grant to institution from General Electric. *Activities not related to the present article:* disclosed no relevant relationships. *Other activities:* disclosed no relevant relation- ships. **C.B.S.** *Activities related to the present article:* disclosed no relevant relationships. *Activities not related to the present article:* board member for AMRA Medical and Guerbet; con- sultant for Boehringer Ingelheim; grants from Gilead, GE Healthcare, Siemens, GE MRI, Bayer AMRI, GE Digital, and GE US; speaker for GE Healthcare and Bayer; educational presentations for Medscape; contracted research for ICON Medical Imaging/Enanta, Philips, Gilead, Shire, Virtualscop- ics, Intercept, and Synageva. *Other activities:* disclosed no rel- evant relationships.

Abstract

The Liver Imaging Reporting and Data System (LI-RADS) stan- dardizes performance of liver imaging in patients at risk for hepa- tocellular carcinoma (HCC) as well as interpretation and reporting of the results. Developed by experts in liver imaging and supported by the American College of Radiology, LI-RADS assigns to obser- vations categories that reflect the relative probability of benignity, HCC, or other malignancy. While category assignment is based mainly on major imaging features, ancillary features may be applied to improve detection and characterization, increase confidence,
or adjust LI-RADS categories. Ancillary features are classified as favoring malignancy in general, HCC in particular, or benignity. Those favoring malignancy in general or HCC in particular may be used to upgrade by a maximum of one category up to LR-4; those favoring benignity may be used to downgrade by a maximum of one category. If there are conflicting ancillary features (ie, one or more favoring malignancy and one or more favoring benignity), the category should not be adjusted. Ancillary features may be seen at diagnostic CT, MRI performed with extracellular agents, or MRI performed with hepatobiliary agents, with the exception of one ancillary feature assessed at US. This article focuses on LI-RADS version 2018 ancillary features seen at MRI. Specific topics include rules for ancillary feature application; definitions, rationale, and il- lustrations with clinical MRI examples; summary of evidence and diagnostic performance; pitfalls; and future directions.

Introduction

Hepatocellular carcinoma (HCC) is the sixth most frequent cancer and second most common cause of mortality attributable to cancer worldwide (1). The majority of HCCs occur in cirrhosis (2,3), most often due to chronic viral hepatitis (4), nonalcoholic fatty liver disease (5,6), and excess alcohol consumption.

Unlike most other cancers, HCC can be diagnosed noninvasively with imaging without mandatory pathology confirmation (7–10). Many diagnostic systems provide algorithms and criteria for imaging-based diagnosis of HCC (11). Among these, the Liver Imaging Reporting and Data System (LI-RADS) has been developed for standardized reporting of imaging results and data collection in patients at risk for HCC. The aims of LI-RADS are to assist radiologists in categorization of liver imaging findings in at-risk patients, diminish imaging interpretation variability, and facilitate communication between radiologists and referring clinicians by using a common terminology. With the support of the American College of Radiology, a committee of radiologists, hepatologists, hepatopathologists, surgeons, and lexicon experts has developed LI-RADS (12) on the basis of scientific evidence, expert opinion, and iterative refinements in response to user feedback (12,13).

The at-risk population targeted by LI-RADS comprises patients with cirrhosis, chronic hepatitis B virus infection without cirrhosis, or current or prior HCC, including adult liver transplant candi- dates and recipients. LI-RADS does not apply to children or to patients with vascular liver disorders or cirrhosis due to congenital hepatic fibrosis. CT and MRI are widely used for diagnosis of HCC. MRI is ideal for characterizing observations using LI-RADS because this modality has numerous contrast enhancement mechanisms and is the only modality that allows assessment of all major as well as ancillary imaging features.

This article focuses on LI-RADS version 2018 ancillary features visible at MRI. It reviews the rules for applying ancillary features; provides defi- nitions and clinical illustrations; summarizes the rationale, evidence, and diagnostic performance supporting the use of ancillary features; and dis- cusses potential pitfalls and future directions.

Categories and Major Features

In LI-RADS, observations are defined as areas with imaging features that differ from those of adjacent liver parenchyma. LI-RADS assigns to imaging- detected liver observations categories that reflect the relative probability of benignity, HCC, or other malignancy. Categories include LR-1 (definitely be- nign), LR-2 (probably benign), LR-3 (intermediate probability for malignancy), LR-4 (probably HCC), LR-5 (definitely HCC), LR-TIV (definite tumor in vein), and LR-M (probably or definitely malignant, not specific for HCC) (Fig 1) (12).

In LI-RADS, major features refer to five imaging features included in the diagnostic table for categorizing LR-3, LR-4, and LR-5 observations: nonrim arterial phase hyperenhancement (APHE), nonperipheral washout appearance (“washout”), enhancing capsule appearance (“capsule”), size, and threshold growth (13). Major features have previously been discussed (13,14) and are not covered in this article.

Ancillary Features

In contrast to major features, ancillary features are optional imaging features applied at the radiolo- gist’s discretion. Ancillary features may be used to improve detection and characterization, increase confidence, or adjust observation category. These ancillary features may favor malignancy in general, HCC in particular, or benignity (Table 1) (12).

Ancillary features favoring malignancy in general or HCC in particular may be used to up- grade by a maximum of one category up to LR-4. Ancillary features that favor malignancy in general can be seen not only in HCC but also in other non-HCC neoplasms such as

cholangiocarcinoma, combined hepatocholangiocarcinoma, or metastases. Ancillary features that favor HCC in particular are more specific for malignancies of hepatocellular origin.

Unlike combinations of major features that can be used to establish a definite diagnosis of HCC (ie, LR-5), ancillary features alone cannot be used to definitely diagnose HCC because they lack the required specificity (15–17).

Studies assessing the clinical application of ancillary features have shown that they modify the final category in 15%–35% of observations (18–20), with about 63% of LR-4 observations being upgraded from LR-3. Use of ancillary features favoring malignancy (including ancillary features favoring HCC in particular) to upgrade LR-3 observations to LR-4 increases sensitivity for HCC (from 87% to 97%) but lowers specificity (from 69% to 51%) at MRI (21). In a separate study, using ancillary features to upgrade LR-3 observations to probable or definite HCC (LR-4, LR-5, or LR-5 V [equivalent to LR-TIV in version 2018]) increased sensitivity (from 76% to 88%) while preserving high specificity (from 88% to 86%) (18).

Ancillary features that favor benignity include size stability for 2 years or longer, size reduction, and features indicative of benign entities. Hence, features that favor benignity reduce the probability of malignancy or HCC. When present, these features are highly specific for benignity (18).

Rules for Application of Ancillary Features

The rules for application of ancillary features are illustrated in Figure 2 and described in this section.

Optional Use of Ancillary Features in LI- RADS Version 2018
Ancillary features are optional, and the decision to use them to adjust observation category is left to the discretion of the radiologist. The optional use of ancillary features allows simplification of the LI-RADS algorithm, resulting in ease of use and wide adoption by new users (16). Nevertheless, radiologists are encouraged to use ancillary features, as these leverage complementary tissue contrast enhancement mechanisms and tumor properties to modulate the final observation category.

Category Upgrade
Ancillary features favoring malignancy in general or HCC in particular may be used to upgrade by one category only and may not be used to upgrade from LR-4 to LR-5. For example, an observation categorized LR-3 may be upgraded to LR-4 in the presence of one or more ancillary features favoring malignancy and in the absence of ancillary features favoring benignity. To preserve high specificity for the LR-5 category, ancillary features may not be used to upgrade observations to LR-5 (12).

Category Downgrade
Ancillary features favoring benignity may be used to downgrade an observation by a maxi- mum of one category. For example, an observation categorized LR-4 may be downgraded to LR-3 in the presence of one or more ancillary features favoring benignity.

Absence of Ancillary Features
The absence of ancillary features should not be used to upgrade or downgrade a category. For example, absence of ancillary features favoring malignancy does not suggest benignity and should not be used to downgrade the category.

Uncertainty
When a radiologist is uncertain about the presence of an ancillary feature, it should be considered absent.

Conflicting Ancillary Features
If there are conflicting ancillary features (ie, one or more favoring malignancy and one or more favoring benignity), the category should not be adjusted. For example, if an LR-3 observation has ancillary features of both malignancy and benignity, the category should remain LR-3.

Ancillary Features Favoring Malignancy in General

Ancillary features favoring malignancy in general can be seen not only in HCC but also in other neoplasms. The ancillary features favoring malignancy in general and their definitions are given in Table 2. The diagnostic performance of ancillary features favoring malignancy in general is summarized in Table 3.

US Visibility as Discrete Nodule

Definition.—US visibility as a discrete nodule refers to visibility at nonenhanced US as a discrete nodule or mass corresponding to a CT- or MRI- detected observation (Fig 3).

Rationale.—The most common benign lesions in the cirrhotic liver (eg, regenerative or low-grade dysplastic nodules) and all benign vascular pseudolesions are typically indistinguishable from the background liver at B-mode US. Hence, lesions visible as discrete nodules are unlikely to be benign. A study revealed that nodules detected at screening US and subsequently seen at CT or MRI were HCCs in a substantial proportion of cases: 69% of LR-3, 96% of LR-4, 98% of LR-5, and 50% of LR-M (40). Because the proportions of HCCs in these LI-RADS categories are higher than for observations discovered with screening US (20), US visibility increases the pretest probability of HCC before characterization with MRI, justifying the use of this ancillary feature to increase confidence and upgrade observation category.

Diagnostic Performance.—The diagnostic performance of US visibility as a discrete nodule, in combination with major features, is unknown. However, the reported per-patient sensitivity and specificity of nonenhanced US in a surveillance setting are 78% and 89%, respectively, according to a meta-analysis by Chou et al (41). The high but imperfect specificity of nonenhanced US alone provides additional justification for US visibility as an ancillary feature.

Subthreshold Growth

Definition.—Subthreshold growth refers to un- equivocal growth of a mass, but less than thresh- old growth. In LI-RADS version 2018, threshold growth is defined as a 50% or greater size increase in 6 months or less. Therefore, subthreshold growth may manifest as a size increase less than 50% in a time interval of 6 months or less, any size increase in a time interval of 6 months or more, or a new observation of any size (Fig 4).

As with threshold growth, subthreshold growth should not be attributable to measurement er- ror or imprecision, differences in technique, or interval hemorrhage. Measurements should be made with the sequence, phase, and plane with which the observation is most clearly visible, us- ing the largest dimension of the observation from outer edge to outer edge, including the "capsule" (when present) and excluding perfusion alterations. The same sequence, phase, and plane of the comparative examination should be used to a ssess interval growth. Measurements in the arterial phase and with diffusion-weighted imaging (DWI) should be avoided because of potential periobservation enhancement and image distor- tion between two sequences, respectively, which may cause measurement error.

Rationale.—Growth rate is usually an indicator of malignancy. Unlike benign observations, which tend to remain stable, grow slowly, or disap- pear, malignant observations grow more rapidly. The growth rate of tumors has typically been reported in terms of tumor volume doubling time (TVDT). The median TVDT is 178 days (about 6 months) for untreated HCC and 82 days (about 3 months) for recurrent HCC after local-regional treatment (13,42). Aggressive and poorly differentiated HCCs tend to grow faster than well-differentiated HCCs.

Growth is not specific to HCC and is observed in other types of tumors as well. Hence, subthresh- old growth is suggestive of malignancy in general, without being specific for HCC. The definition of subthreshold growth is adapted from the definition of threshold growth (a major feature), itself based on a combination of expert opinion and desire to maintain congruency with the OPTN/UNOS (Organ Procurement and Transplantation Network/ United Network for Organ Sharing) definition of growth for prioritization of liver transplantation in HCC patients. As described earlier, threshold growth is defined in LI-RADS version 2018 as ≥50% or greater size increase of a mass in 6 months or less. Size should be measured with the same sequence, phase, and plane in serial examinations.

Diagnostic Performance.—According to one study (18), subthreshold growth as a stand-alone feature has sensitivity of 48% and specificity of 91% for diagnosis of HCC. The incremental effect on diagnostic performance of subthreshold growth in combination with major features is unknown. Although retrospective and prospective studies are lacking, indirect evidence and biologic plausibility suggest that subthreshold growth favors malignancy (13).

Corona Enhancement

Definition.—Corona enhancement refers to periobservation enhancement in the late arterial or early portal venous phase (PVP) attributable to venous drainage from the tumor (Fig 5).

Rationale.—Also called peritumoral enhancement or corona stain, corona enhancement is reported in 60%–81% of HCCs at MRI (21,43). Corona enhancement is not a feature of early and small HCC and is more often seen in hypervascular progressed HCC. This transient imaging feature is caused by venous drainage of contrast material from the tumor into the peritumoral parenchymal sinusoids and portal venules. This ab- errant and disorganized venous drainage develops during hepatocarcinogenesis owing to occlusion of intranodular hepatic veins (44–48).

This ancillary feature has diagnostic value, as it can help differentiate tumors such as HCC from benign vascular pseudolesions, which do not manifest a corona. The feature is associated with microvascular invasion (49) and so has prognostic value for predicting the presence of such invasion. Additionally, since many intra- hepatic metastases (ie, seeding of daughter or satellite nodules) form in the peritumoral venous drainage area (47,50), the corona enhancement territory should be included within the surgical margin and in the ablation zone to reduce the risk of local recurrence after hepatectomy and local-regional treatment, respectively (50).

Corona enhancement can also be seen in liver metastases with peritumoral neovascularization and inflammatory changes (51). Therefore, this ancillary feature favors malignancy in general and is not specific for HCC. Corona enhancement around HCCs and other malignant lesions may overlap in appearance with arterioportal shunting, which can occur with both benign and malignant lesions. Distinguishing features are that corona enhancement tends to be confined to the immediate peritumoral parenchyma, ap- pears in the late arterial phase, and then fades to isoenhancement, whereas arterioportal shunting tends to encompass a broader area and peaks in intensity in the early arterial phase (48,52). Co-rona enhancement should also be distinguished from an enhancing “capsule,” which is seen as a smooth, uniformly thick, and progressively enhancing rim of tissue that appears during the portal venous, delayed, or transitional phase.

Diagnostic Performance.—The incremental effect on diagnostic performance of corona enhancement in combination with major features is unknown.

Fat Sparing in Solid Mass

Definition.—Fat sparing in a solid mass refers to relative paucity of lipid in a solid mass compared with steatotic liver or in an inner nodule relative to a steatotic outer nodule (Figs 6, 7). This feature applies only to patients with steatotic tissue—either a steatotic liver or steatotic nodules. Steatotic tissue can be recognized at gradient-echo imaging when there is signal drop on out-of-phase images in comparison with in-phase images. Fat sparing in a solid mass is seen as absence of or lesser signal drop in an observation relative to its surroundings.

Rationale.—Evidence supporting this feature is indirect. Pathology studies have shown that progressed HCCs are rarely steatotic (the exception is steatohepatic variant), whereas early HCCs and dysplastic nodules are frequently steatotic. Additionally, fat accumulation does not occur in cholangiocarcinoma and other non-HCC malignancies (53). Therefore, the evidence that supports using fat sparing in a solid mass as a feature in favor of malignancy remains indirect (16).

Perfusional alteration and diffuse heterogeneous fatty infiltration of the liver may be associated with areas of fat sparing, which must not be mistaken for lesional fat sparing. Typical focal fat sparing occurs around the gallbladder and hepatic hilum, resulting from direct splanchnic venous supply reduced in lipid compared with portal flow, at the posterior edge of segment II/III from an aberrant left gastric vein or at the posterior edge of segment IV caused by aberrant right gastric vein drainage (54).

Diagnostic Performance.—The incremental effect on diagnostic performance of fat sparing in a solid mass in combination with major features is unknown.

Restricted diffusion

Definition.—Restricted diffusion refers to in- creased signal intensity at DWI, not attributable solely to T2-weighted imaging shine-through, unequivocally higher than in liver and/or apparent diffusion coefficient (ADC) unequivocally lower than in liver parenchyma (Fig 8). DWI is optional in LI-RADS technical recommendations. Although there is no consensus on the optimal b values for diagnosing HCC in cirrhosis (55), DWI should include low b values (≤50 sec/mm^2) and high b values (≥400 sec/mm^2) (12,56).

Rationale.—Malignant tumors have higher cellular density and nucleus-to-cytoplasm ratio, leading to reduction in extracellular and intracellular space, respectively. This high cellularity restricts the motion of water molecules. DWI, a form of phase-contrast imaging to encode the diffusion of water molecules, can leverage this physical concept to provide information on tissue cellularity: diffusion is relatively unrestricted in normal tissue and restricted in tumors. However, unlike normal liver, cirrhotic liver has excess collagen in the extracellular matrix, which is thought to impede the diffusion of water. Hence, cirrhotic liver may have higher than normal signal intensity at DWI, potentially limiting the visibility of focal lesions (57,58).

Hypovascular nodules that become hyper- intense at follow-up DWI have higher risk of transformation to hypervascular HCCs (59). DWI may help differentiate chronic bland thrombus from tumor in vein (60), but this technique does not allow reliable differentiation of acute bland thrombus, which also may manifest with impeded diffusion. Some studies have found that the ADC correlates to the degree of differentiation of HCCs (61,62). However, there is overlap between the ADC of benign and malignant solid tumors, which leads to variations in diagnostic thresholds reported for characterization of lesions. Further, a major barrier to application of ADC thresholds is lack of standardization of DWI protocols and measurement techniques (63).

Diagnostic Performance.—Hyperintensity at DWI (b ≥ 500 sec/mm^2) combined with contrast-en- hanced MRI increases sensitivity for HCC versus dysplastic nodule from 68% to 98% and accuracy from 76% to 93% (24). Hyperintensity at DWI (b ≥ 500 sec/mm^2) as an incremental feature to major features (APHE and washout) increases sensitivity for diagnosis of histologically proved HCC from 60%–62% to 70%–80% (64).

Mild-Moderate T2 Hyperintensity

Definition.—Mild-moderate T2 hyperintensity refers to signal intensity at T2-weighted imaging that is mildly or moderately higher than that of the liver and similar to or less than that of non– iron-overloaded spleen parenchyma (Fig 9). This increased signal intensity is less than that of fluid (ie, less than that of cerebrospinal fluid if taken as a comparative background).

Rationale.—T2 hyperintensity may reflect intratumoral dilated sinusoids (65), edema, or watery fibrosis (66). Regenerative nodules and dysplastic nodules are rarely hyperintense to surrounding liver parenchyma at T2-weighted imaging (35,67–69) unless infarcted (70) or in patients with Budd-Chiari syndrome (71). How- ever, T2 hyperintensity is seen in 42%–47% of HCCs (28,72). Hence, T2 hyperintensity of an observation, compared with background liver, in addition to dynamic imaging, may help differentiate small (≤2 cm) HCCs from benign nodules (22) and hypervascular pseudolesions (73), as well as hypovascular HCCs from dysplastic nodules (23). However, T2 hyperintensity is not specific for HCC, as it may be seen in other malignancies (53).

The level of T2 hyperintensity is correlated with HCC size (74), degree of hypervascularity (75), growth rate (76), and progression from early to well-differentiated HCC (77–79). T2 hyperintensity also constitutes a risk factor for growth and development of APHE in a nodule that is initially hypovascular (80).

Diagnostic Performance.—Mild-moderate T2 hyperintensity, when used in combination with DWI, has sensitivity of 72% and specificity of 100% for distinguishing hypovascular HCC from a dysplas- tic nodule. Mild-moderate T2 hyperintensity has a weak incremental effect on diagnostic performance because it is more often seen in progressed HCCs and therefore in association with other major or ancillary features (28,53,72).

Iron Sparing in Solid Mass

Definition.—Iron sparing in a solid mass refers to a paucity of iron in an inner nodule compared with a siderotic outer nodule or to a solid mass containing less iron relative to iron-overloaded background liver (Fig 10). Iron overload in the liver can be primary (genetic) or secondary (due to exogenous iron administration) (81). At gradient-echo imaging, iron-overloaded tissue shows decreased signal intensity on images with longer echo time (TE) (typically the in-phase images compared with the out-of-phase images when using a dual-echo gradient-echo sequence). This is because the superparamagnetic effect of iron particles (ferritin and hemosiderin) shortens the transverse relaxation constants, resulting in a decrease in signal intensity of the iron-containing tissue. Solid masses with iron sparing show less signal loss than the siderotic outer nodule or the iron-overloaded background liver on the second echo of a dual-echo sequence.

Rationale.—Low-grade dysplastic nodules in cir- rhotic liver tend to accumulate iron and appear T2 or T2* hypointense compared with the remaining parenchyma, presumably reflecting iron avidity by the dysplastic but nonmalignant cells. By com- parison, malignant hepatocytes lose their ability to accumulate iron and become “iron-resistant” (82–84). Studies have described development of HCC foci in dysplastic nodules as a nodule-in-nodule appearance recognizable as a T2-isointense spot in a low-signal-intensity nodule, representing an iron-free HCC focus within a larger siderotic nodule (82,83,85). In patients with hemochro- matosis, iron-free nodules have been shown to be premalignant (86,87).

Iron sparing in a solid mass favors malignancy but is not specific for HCC, as it may also be observed in intrahepatic cholangiocarcinoma or other non-HCC malignancies (53). Confluent fibrosis is also iron-free; however, it should not be mistaken for iron sparing in a solid mass because areas of fibrosis have an elongated, linear, branching, or wedgelike configuration, with associated capsular retraction (16,53).

Diagnostic Performance.—The incremental effect on diagnostic performance of iron sparing in a solid mass in combination with major features is unknown. Although retrospective and prospective studies are lacking, indirect evidence and biologic plausibility suggest that iron spar-ing in a solid mass favors malignancy.

Transitional Phase Hypointensity

Definition.—Transitional phase hypointensity of an observation refers to signal intensity in the transitional phase unequivocally less, in whole or in part, than in the liver (Figs 11, 12). The transi-tional phase is the postcontrast phase performed 3–5 minutes after injection of gadoxetate disodium. It occurs after the extracellular phase (ie, after the PVP) and before the hepatobiliary phase (HBP); hence, the transitional phase may begin as early as 2 minutes after injection.

As a pure equilibrium phase does not exist with hepatobiliary agents, the transitional phase represents the period of transition in which parenchymal enhancement may be attributable to the presence of contrast agent in both the extracellular and intracellular compartments (88). During the transitional phase, liver vessels and hepatic parenchyma are of similar signal inten- sity. Interpretation of signal intensity during the transitional phase can be challenging, as hyper- enhancement of liver parenchyma may give the impression of de-enhancement of the mass (53).

Rationale.—Transitional phase hypointensity is reported in 47%–65% of HCCs (31,35) and is thought to reflect a combination of mechanisms including "washout" and underexpression of organic anion-transporting polypeptide (OATP), the membrane transporter responsible for uptake by hepatocytes of these agents. Transitional phase hypointensity is sensitive but not specific for HCC and may be seen in any mass devoid of the molecular transporters, including cholangiocarcinoma, metastases, and hemangioma (76). Therefore, transitional phase hypointensity alone cannot be used to diagnose HCC.

Diagnostic Performance.—When used in com- bination with PVP "washout," transitional phase hypointensity has sensitivity of 83%–91% and specificity of 33%–58% for histopathologically confirmed HCC (31).

HBP Hypointensity

Definition.—HBP hypointensity refers to signal intensity in the HBP unequivocally less, in whole or in part, than in the liver (Fig 13). The HBP is the postcontrast phase performed with a hepatobiliary agent in which the liver parenchyma is hyperintense to hepatic blood vessels and there is excretion of contrast material into the biliary system. The HBP is typically performed 20 minutes after injection with gadoxetate disodium (89) and 1–3 hours after injection with gadobenate dimeglumine. The HBP is suboptimal if the liver is not more intense than the hepatic blood vessels. The presence of biliary excretion is not an indicator of an adequate HBP.

Rationale.—Hepatobiliary contrast agents provide an additional tissue contrast mechanism to characterize liver observations. OATP expression decreases during hepatocarcinogenesis, resulting in HBP hypointensity of both early and progressed HCCs (90). HBP hypointensity is reported in 79%–99% of HCCs (39,91,92).

Addition of the HBP when using a hepato- biliary contrast agent increases sensitivity by 5%–19% for diagnosis of HCC (33,34,37,93,94) because HBP hypointensity occurs before the onset of arterialization in hepatocarcinogenesis (95). Hence, HBP hypointensity can reveal early HCCs that are hypovascular (35) or indeterminate in

dynamic phases alone because of their atypical features (34). HBP hypointensity may help differentiate early HCCs and high-grade dysplastic nodules from low-grade dysplastic nodules (35,38). HBP hypointensity is sensitive but not specific for diagnosis of HCC because non-HCC malignancies and benign entities such as hemangioma are devoid of OATP and typically appear hypointense in the HBP.

Diagnostic Performance.—HBP hypointensity used in combination with major features has sensitivity of 75%–99% (32,34) and specificity of 42%–96% (32,35,38,39).

Ancillary Features Favoring HCC in Particular

Ancillary features favoring HCC in particular and their definitions are given in Table 4. Estimates of diagnostic performance are not available for these ancillary features.

Nonenhancing "Capsule"

Definition.—Nonenhancing "capsule" refers to a capsule appearance that is not visible as an enhancing rim (Fig 14). This feature can appear as a hypointense rim on T2-weighted, nonenhanced T1-weighted, or HBP images. Nonenhancing "capsule" should be unequivocally thicker or more conspicuous than fibrotic tissue around background nodules.

Distinction should be made from targetoid appearance and peripheral "washout," which are both features of non-HCC malignancies (LR- M). Targetoid appearance in the PVP or HBP is a concentric pattern characterized by moderate to marked hypointensity in the periphery of the observation with milder hypointensity in the center. Peripheral "washout" is a spatially defined subtype of "washout" in which apparent wash- out is most pronounced in the periphery of the observation (12). In both cases, the pitfall can be avoided by assessing the entire dynamic phases.

Rationale.—A radiologically identified "capsule" may represent a pseudocapsule comprising perile- sion sinusoids, fibrous tissue, and compressed liver parenchyma. The distinction between a true tumor capsule and pseudocapsule can be made only at pathologic analysis, but this distinction does not appear important for diagnosing HCC or evaluating its biologic behavior. Unlike enhancing "cap- sule," nonenhancing "capsule" does not appear as an enhancing rim. The presence of a hypointense rim in the HBP, a subtype of nonenhancing "capsule," may be due to peritumor hypoperfusion from obstructed intrahepatic portal flow and insufficient hepatic arterial supply, leading to liver parenchyma injury and subsequent decreased uptake of gadoxetate disodium (96).

Diagnostic Performance.—The incremental effect on diagnostic performance of nonen- hancing "capsule" in combination with major features is unknown.

Mosaic Architecture

Definition.—Mosaic architecture refers to the presence of randomly distributed internal nod- ules or compartments, usually with different imaging features (Fig 15). Internal compartments may differ because of the presence of fat, fibrosis, blood products, and vascular dynamics. Heterogeneity of compartments in mosaic appearance is better depicted on T2-weighted images than on T1-weighted images (65).

Rationale.—Mosaic pattern is seen in 28%–63% of cases (17), more commonly in HCCs than in non-HCCs (97) and more frequently in large HCCs (>3 cm) (98). Mosaic appearance at imaging corresponds to the appearance at histopathologic examination (99). Multiple nodules or masses within a larger mass correspond to different foci of clonal expansion at different stages of hepatocarcinogenesis (16,17,100), some of which may contain fat metamorphosis, separated by areas of necrosis, blood products, cystic

degeneration, and fibrous septa. Nodular areas that demonstrate APHE typically have higher histologic grade than hypovascular areas, which are supplied by portal venous flow. Mosaic appearance is unusual in non-HCC malignancy (53) and therefore favors HCC in particular.

Diagnostic Performance.—The incremental effect on diagnostic performance of mosaic architecture in combination with major features is unknown.

Nodule-in-Nodule Architecture

Definition.—Nodule-in-nodule architecture refers to the presence of a smaller inner nodule within and having different imaging features than the larger outer aspect of the entire nodule (Fig 16). Imaging features can differ in terms of signal intensity and/or enhancement.

Rationale.—Nodule-in-nodule architecture ap- pears at MRI as a central focus of HCC within a large dysplastic nodule (85). This imaging feature corresponds to the characteristic histologic growth pattern of hepatocarcinogenesis: morpho- logic dedifferentiation and clonal multiplication of less-differentiated cells in the inner nodule re- placing the well-differentiated or dysplastic outer nodule (101,102). During hepatocarcinogenesis, inner foci of HCC may become iron-resistant (82,83), accumulate fat (35), or become hyperar- terialized (103,104). The inner nodule may thus appear T2 isointense or hyperintense (68,85), show signal drop on out-of-phase images, or
demonstrate APHE (35,105). Necrotic HCCs with inner nodules of viable tumor may also demonstrate nodule-in-nodule architecture (105).

The inner HCC focus demonstrates marked TVDT of 9.5 weeks and potential for rapid growth (106). Measurement of observation size should be made on the entire observation, including the larger outer nodule and smaller inner nodule. As it is characteristic of hepatocarcinogenesis but does not occur with other malignant tumors such as cholangiocarcinoma, nodule-in- nodule appearance favors HCC in particular.

Diagnostic Performance.—The diagnostic performance of nodule-in-nodule architecture, as a stand-alone feature or in combination with major features, is unknown.

Fat in Mass, More than in Adjacent Liver

Definition.—Fat in a mass, more than in adjacent liver, refers to excess fat within a mass, in whole or in part, relative to adjacent liver (Fig 17). Intracellular fat in HCCs can be diagnosed at MRI as a drop in signal intensity of a mass on opposed-phase gradient-echo images compared with in-phase images.

Rationale.—Fatty metamorphosis in HCCs is not fully understood. Some authors have speculated that it arises in high-grade dysplastic nodules and early HCCs in response to tumor hypoxia caused by destruction of intranodule portal tracts and incomplete neoarterialization. Once unpaired arteries develop in progressed HCCs, the hypoxia resolves and the steatosis regresses, explaining why fat deposition is infrequent in progressed and large HCCs (107). The mechanism by which hypoxia would induce fat accumulation is unclear. Another hypothesis for intralesion fatty metaplasia is clonal proliferation of hepatocytes with dysregulated lipogenesis (108).

Although fat in a mass can be found in premalignant hepatocellular lesions such as high-grade dysplastic nodules (109), it is rarely found in non- HCC malignancies such as cholangiocarcinoma (110) and therefore is considered a feature favoring HCC. However, the presence of fat in a mass should not modify the observation category if other imaging features (ie, targetoid appearance) indicate LR-M, since hepatocholangiocarcinomas may

contain fat within their hepatocellular component. Other liver masses such as adenoma, angiomyolipoma, teratoma, or metastases from liposarcoma or renal cell carcinoma may also contain fat (17) but are exceptionally rare in cirrhotic livers (111). Intralesion fat should not be confused with focal liver steatosis or fat drops after transarterial chemo-embolization with an oil-containing agent (Lipiodol [ethiodized oil]; Guerbet, Villepinte, France).

Diagnostic Performance.—Fat in a mass, more than in adjacent liver, is observed in 16%–18% of HCCs (112,113). However, the incremental contribution of this ancillary feature to overall diagnostic performance may be limited because fat in a mass, more than in background liver, does not allow reliable distinction of early HCCs from high-grade and even low-grade dysplastic nod- ules and often coexists in progressed HCCs with the hallmark enhancement pattern of APHE and "washout" (113).

Blood Products in Mass

Definition.—Blood products in a mass refers to intralesion or perilesion hemorrhage in the absence of biopsy, trauma, or intervention (Fig 18). Acute or subacute blood products appear hyperintense on T1-weighted images (owing to intracellular or extracellular methemoglobin) and hyperintense and heterogeneous on T2-weighted images (owing to extracellular methemoglobin), while chronic blood products appear hypointense with both SE quences (owing to hemosiderin). The scavenging of methemoglobin into hemosiderin by macro- phages occurs at the periphery of the hematoma, hence there is a peripheral hypointense rim on T2*-weighted images. Blood products that are hyperintense on T1-weighted images may obscure assessment of APHE (or enhancement in any phase). In such cases, a vascular subtraction series may be helpful.

Rationale.—HCCs are hypervascular tumors prone to hemorrhage. Spontaneous intralesion bleeding is reported in up to 19% of HCCs (114). Postulated mechanisms include repetitive minor blunt trauma to superficial lesions, rapid elevation in intratumor pressure caused by thrombosis of draining veins, and rupture of fragile neoarteries in the tumor (115).

Bleeding in HCC can be minor and contained within the tumor or may rupture through the tumor into the surrounding liver or the subcapsular space of the liver or even through the liver capsule into the peritoneum. Although hepatocellular adenomas and some hepatic metastases may manifest with bleeding, these tumors are exceptionally rare in cirrhotic patients (115). Other tumors such as cholangiocarcinoma are not prone to hemorrhage.

Diagnostic Performance.—The incremental ef- fect on diagnostic performance of blood products in a mass in combination with major features is unknown. Indirect evidence and biologic plausibil-ity suggest that blood products in an observation strongly favor HCC in particular.

Ancillary Features Favoring Benignity Ancillary features favoring benignity are given in Table 5. The diagnostic performance of ancil- lary features favoring benignity is summarized in Table 6.

Size Stability for 2 Years or Longer

Definition.—Size stability for 2 years or longer is defined as absence of significant change in an observation's size when measured at examinations 2 years or longer apart and in the absence of treat- ment (Fig 19). Size stability should be assessed between two examinations with measurements using the same sequence, phase, and plane.

Rationale.—The reported TVDT of HCC varies from 12 to 851 days (2.3 years) (49,118) depend- ing on the degree of dedifferentiation. The TVDT of cholangiocarcinoma in cirrhotic liver is un- known, but a median TVDT of 70 days has been reported in a noncirrhotic patient (119). Precursor nodules evolving into HCCs have a reported aver-age TVDT of 5.3 months (76). Therefore, absence of growth for 2 years or longer would be unusual for HCC or another malignant entity in cirrhotic patients and hence size stability favors benignity.

Diagnostic Performance.—The incremental effect on diagnostic performance of size stability for 2 years or longer in combination with major features is unknown. Indirect evidence and bio- logic plausibility suggest that size stability for 2 years or longer favors benignity.

Size Reduction

Definition.—Size reduction refers to unequivocal spontaneous decrease in size of an observation over time unattributable to artifact, measurement error, technique differences, or resorption of hemorrhage (Fig 20).

Rationale.—Malignant tumors are the result of cel-lular clonal multiplication and therefore grow overtime. Spontaneous regression of HCC is rare: only75 cases of spontaneous regression of HCC have been reported as of 2012 (120,121). Postulated mechanisms include tumor ischemia and necrosis induced by rapid growth and immune response against tumor cells triggered by an otherwise unrelated bacterial infection, although the cause ofregression is unknown in one-half of cases (120). By comparison, hemangiomas in the cirrhotic livertend to involute and eventually disappear as a resultof progressive intralesion fibrosis (122).

Because spontaneous regression of HCC orother malignant entities is rare and because size reduction can be observed in benign entities suchas hemangiomas, this ancillary feature favors a benign entity. However, size reduction due to resorption of blood products from a hemorrhagicHCC (Fig 21) constitutes a pitfall and should notbe interpreted as favoring benignity.

Diagnostic Performance.—The incremental effecton diagnostic performance of size reduction in combination with major features is unknown. Indirect evidence and biologic plausibility suggest that size reduction favors benignity.

Parallels Blood Pool Enhancement

Definition.—Parallels blood pool enhancement refers to a temporal pattern in which enhancement ventually reaches and then matches that of the blood pool (ie, enhancement similar to that of ar- terial structures in the arterial phase and the portalvein or inferior vena cava in the PVP, delayed phase, transitional phase, and HBP) (Fig 22).

Rationale.—Enhancement that parallels the bloodpool is a typical feature of hemangioma (123) and has been attributed to puddling of contrast mate- rial within the large endothelium-lined vascular channels. The level of enhancement of hemangio- mas approximates that of the blood pool vein in allvascular phases. However, the blood pool becomesdark relative to the liver after the transitional phase using hepatobiliary agents, which may causediagnostic confusion (123,124). In addition to hemangiomas, this temporal enhancement patternmay also be seen in observations that have direct communication with vascular structures, such as pseudoaneurysms and arteriovenous fistulas.

In contrast, HCCs typically demonstrate APHEand/or “washout” at dynamic imaging and metastases demonstrate targetoid enhancement (117). One pitfall is peliotic HCC, a rare HCC variant with dilated intratumor sinusoids. Enhancement in this type of HCC may also parallel the blood poolowing to puddling of contrast material within the dilated sinusoids (125).

Diagnostic Performance.—The diagnostic performance of blood pool parallelism, in the ab-sence of the characteristic morphologic pattern,is unknown.

Undistorted Vessels

Definition.—Undistorted vessels refers to vessels traversing an observation without displacement, deformation, or other alteration (Fig 23).

Rationale.—Vessels traversing an observation without any alteration of their path exclude the presence of mass effect. Perfusion alterations, areas of fat deposition, and hypertrophic pseudomasses do not exert mass effect and therefore do not distort traversing vessels. In contrast, tumors are space-occupying lesions displacing or distorting vessels and surrounding parenchyma. Therefore, undistorted vessels indicate absence of an underlying mass and are a feature favoring benignity.

Diagnostic Performance.—The incremental effect on diagnostic performance of undistorted vessels in combination with major features is unknown.

Indirect evidence and biologic plausibility suggest that undistorted vessels favor benignity.

Iron in Mass, More than in Liver

Definition.—Iron in a mass, more than in the liver, refers to excess iron in a mass relative to that in background liver. At gradient-echo imaging, iron-rich nodules show decreased signal intensity on images with longer echo time (ie, on the in-phase images) owing to shortening of transverse relaxation constants by the superparamagnetic effect of iron.

Rationale.—Iron-rich nodules, also known as siderotic nodules, are frequent in the cirrhotic liver. These lesions are usually benign low-grade dysplastic nodules; they are rarely high-grade or malignant lesions. An increased prevalence of HCC in siderotic nodules has not been demon- strated (126). For these reasons, the presence of iron favors benignity. However, the presence of blood degradation products and accumulation of hemosiderin that may be seen in hemorrhagic HCCs (Fig 24) constitutes a pitfall and should not be interpreted as a feature favoring benignity.

Diagnostic Performance.—The incremental effect on diagnostic performance of iron in a mass in combination with major features is unknown. Indirect evidence and biologic plausibility sug- gest that iron in a mass favors benignity.

Marked T2 Hyperintensity

Definition.—Marked T2 hyperintensity refers to signal intensity of an observation on T2-weighted images markedly higher than that of the liver and similar to that of the bile ducts and other fluid-filled structures (Fig 25).

Rationale.—Marked T2 hyperintensity cor- responds to the signal intensity of liquid and is more accentuated on heavily T2-weighted mages with longer TEs. This ancillary feature is observed in benign fluid-filled structures such as liver cysts, hamartomas, biliary structures, and abscesses (127) or with slow-flowing blood in hemangiomas (123). Hepatic cystic neoplasms, such as cystadenoma or cystadenocarcinoma, or necrotic metastases may exhibit marked T2 hyperintensity in association with multiple septa or a rim of peripheral solid tissue, but these neoplasms are rare in cirrhosis. Except in areas of necrosis, HCCs seldom manifest with marked T2 hyperintensity.

Diagnostic Performance.—Marked T2 hyper- intensity on heavily T2-weighted images allows distinction of hemangiomas from HCCs and other malignant solid lesions with sensitivity of 75%–80% and specificity of 85%–100% (116,128).

HBP Isointensity

Definition.—HBP isointensity refers to signal in- tensity of an observation in the HBP nearly identi-cal to that of the background liver (Fig 26).

Rationale.—As mentioned earlier, most HCCs and virtually all other malignancies have reduced for absent expression of OATP and therefore tend to appear hypointense in the HBP. Isointensity relative to the liver in the HBP indicates the presence of functional hepatocytes with preserved OATP expression, typically seen in regenerative nodules, low-grade dysplastic nodules (129,130), and benign arterioportal shunts (39,131). However,

HBP isointensity does not completely exclude malignancy, as 2.5%–8.5% of HCCs may appear iso- or hyperintense relative to the surrounding parenchyma in the HBP (129). HCCs that are iso- or hyperintense in the HBP tend to be more indolent and have a more favorable prognosis (53,132).

Diagnostic Performance.—HBP isointensity in combination with major features has sensitivity of91%–94% and specificity of 93% for differentiating arterioportal shunt from HCC (39).

Future Directions

Ancillary features have been defined on the basis of imaging features described in the radiology literature. Evidence of the diagnostic accuracy and reproducibility of ancillary features—alone and in combination with other features—remains scarce. Further research is required to assess thediagnostic performance of ancillary features and determine their relative weights. Pooling of data from multiple centers may be required.

Further research is also needed to better understand the frequency with which ancillary features affect LI-RADS categorization when used in combination with major features (Figs 27, 28) as well as their effect on improving lesiondetection.

Conclusion

MRI is frequently used for definitive and non- invasive diagnosis of HCC without mandatory histopathologic confirmation. Ancillary features are based on biologic and physical concepts described in the radiology literature. Although optional, use of ancillary features may improve confidence in the LI-RADS category, modify the observation category, or increase sensitivity for diagnosis of HCC. In this article, we provide the definitions for, review the rationale behind, and summarize the diagnostic performance of ancillary features favoring malignancy in general, favoring HCC in particular, or favoring benignity. Further research is needed to validate their ap- plication and inform their refinement.

References

1. Mittal S, El-Serag HB. Epidemiology of hepatocellular carcinoma: consider the population. J Clin Gastroenterol 2013;47(suppl):S2–S6.
2. Llovet JM, Burroughs A, Bruix J. Hepatocellular carcinoma. Lancet 2003;362(9399):1907–1917.
3. El-Serag HB. Hepatocellular carcinoma. N Engl J Med 2011;365(12):1118–1127.
4. El-Serag HB. Epidemiology of viral hepatitis and he- patocellular carcinoma. Gastroenterology 2012;142(6): 1264–1273 e1.
5. N oureddin M, Rinella ME. Nonalcoholic fatty liver disease, diabetes, obesity, and hepatocellular carcinoma. Clin Liver Dis 2015;19(2):361–379.
6. Pocha C, Kolly P, Dufour JF. Nonalcoholic fatty liver disease–related hepatocellular carcinoma: a problem of growing magnitude. Semin Liver Dis 2015;35(3): 304–317.
7. Bruix J, Sherman M; American Association for the Study of Liver Diseases. Management of hepatocellular carci- noma: an update. Hepatology 2011;53(3):1020–1022.
8. OPTN/UNOS policy 9: allocation of livers and liver-intes- tines. https://optn.transplant.hrsa.gov/ContentDocuments/ OPTN_Policies.pdf-nameddest=Policy_09. Published 2015. Accessed April 26, 2018.
9. European Association for the Study of the Liver; European Organisation for Research and Treatment of Cancer. EASL-EORTC clinical practice guidelines: manage- ment of hepatocellular carcinoma. J Hepatol 2012;56(4):908–943.
10. AASLD guideline policies, including the AASLD policy on the development and use of practice guidelines and the American Gastroenterology Association policy statement on guidelines. http://www3.aasld.org/practiceguidelines/ Documents/Policy on Development.pdf. Published 2009. Accessed April 26, 2018.
11. Tang A, Cruite I, Mitchell DG, Sirlin CB. Hepatocellular carcinoma imaging systems: why they exist, how they have evolved, and how they differ. Abdom Radiol (NY) 2018;43(1):3–12.
12. American College of Radiology. Liver Imaging Reporting and Data System version 2018. https://www.acr.org/Clinical- Resources/Reporting-and-Data-Systems/LI-RADS. Accessed July 30, 2018.
13. Tang A, Bashir MR, Corwin MT, et al. Evidence supporting LI-RADS major features for CT- and MR imaging–based diagnosis of hepatocellular carcinoma: a systematic review. Radiology 2018;286(1):29–48.
14. Elsayes KM, Hooker JC, Agrons MM, et al. 2017 version of LI-RADS for CT and MR imaging: an update. Radio- Graphics 2017;37(7):1994–2017.
15. Cruite I, Tang A, Mamidipalli A, Shah A, Santillan C, Sirlin CB. Liver Imaging Reporting and Data System: review of major imaging features. Semin Roentgenol 2016;51(4): 292–300.
16. Chernyak V, Tang A, Flusberg M, et al. LI-RADS® ancillary features on CT and MRI. Abdom Radiol (NY) 2018;43(1):82–100.
17. Khatri G, Merrick L, Miller FH. MR imaging of hepatocel- lular carcinoma. Magn Reson Imaging Clin N Am 2010;18(3):421–450, x.
18. Cerny M, Bergeron C, Billiard JS, et al. LI-RADS for MR imaging diagnosis of hepatocellular carcinoma: performance of major and ancillary features. Radiology 2018;288(1):118–128.
19. Joo I, Lee JM, Lee DH, Ahn SJ, Lee ES, Han JK. Liver Imaging Reporting and Data System v2014 categorization of hepatocellular carcinoma on gadoxetic acid-enhanced MRI: comparison with multiphasic multidetector com- puted tomography. J Magn Reson Imaging 2017;45(3): 731–740.
20. Choi SH, Byun JH, Kim SY, et al. Liver Imaging Report- ing and Data System v2014 with gadoxetate disodium- enhanced magnetic resonance imaging: validation of LI-RADS category 4 and 5 criteria. Invest Radiol 2016;51(8):483–490.
21. Ronot M, Fouque O, Esvan M, Lebigot J, Aubé C, Vilgrain V. Comparison of the accuracy of AASLD and LI-RADS criteria for the non-invasive diagnosis of HCC smaller than 3 cm. J Hepatol 2017 Dec 21. pii: S0168-8278(17)32529-1 [Epub ahead of print].
22. Kwon HJ, Byun JH, Kim JY, et al. Differentiation of small (≤2 cm) hepatocellular carcinomas from small benign nodules in cirrhotic liver on gadoxetic acid-enhanced and diffusion-weighted magnetic resonance images. Abdom Imaging 2015;40(1):64–75.
23. Hwang J, Kim YK, Jeong WK, Choi D, Rhim H, Lee WJ. Nonhypervascular hypointense nodules at gadoxetic acid– enhanced MR imaging in chronic liver disease: diffusion-weighted imaging for characterization. Radiology 2015; 276(1):137–146.
24. Xu PJ, Yan FH, Wang JH, Shan Y, Ji Y, Chen CZ. Contri- bution of diffusion-weighted

magnetic resonance imaging in the characterization of hepatocellular carcinomas and dysplastic nodules in cirrhotic liver. J Comput Assist Tomogr 2010;34(4):506–512.
25. Inchingolo R, De Gaetano AM, Curione D, et al. Role of diffusion-weighted imaging, apparent diffusion coefficient and correlation with hepatobiliary phase findings in the differentiation of hepatocellular carcinoma from dys- plastic nodules in cirrhotic liver. Eur Radiol 2015;25(4): 1087–1096.
26. Granata V, Fusco R, Avallone A, et al. Critical analysis of the major and ancillary imaging features of LI-RADS on 127 proven HCCs evaluated with functional and morpho- logical MRI: lights and shadows. Oncotarget 2017;8(31): 51224–51237.
27. Le Moigne F, Durieux M, Bancel B, et al. Impact of diffusion-weighted MR imaging on the characterization of small hepatocellular carcinoma in the cirrhotic liver. Magn Reson Imaging 2012;30(5):656–665.
28. Hecht EM, Holland AE, Israel GM, et al. Hepatocellular carcinoma in the cirrhotic liver: gadolinium-enhanced 3D T1-weighted MR imaging as a stand-alone sequence for diagnosis. Radiology 2006;239(2):438–447.
29. Kim JE, Kim SH, Lee SJ, Rhim H. Hypervascular hepato- cellular carcinoma 1 cm or smaller in patients with chronic liver disease: characterization with gadoxetic acid-enhanced MRI that includes diffusion-weighted imaging. AJR Am J Roentgenol 2011;196(6):W758–W765.
30. Ouedraogo W, Tran-Van Nhieu J, Baranes L, et al. Evalu- ation of noninvasive diagnostic criteria for hepatocellular carcinoma on pretransplant MRI (2010): correlation between MR imaging features and histological features on liver speci- men [in French]. J Radiol 2011;92(7-8):688–700.
31. Joo I, Lee JM, Lee DH, Jeon JH, Han JK, Choi BI. Nonin- vasive diagnosis of hepatocellular carcinoma on gadoxetic acid-enhanced MRI: can hypointensity on the hepatobili- ary phase be used as an alternative to washout? Eur Radiol 2015;25(10):2859–2868.
32. Di Martino M, Anzidei M, Zaccagna F, et al. Qualitative analysis of small (≤2 cm) regenerative nodules, dysplastic nodules and well-differentiated HCCs with gadoxetic acid MRI. BMC Med Imaging 2016;16(1):62.
33. Ahn SS, Kim MJ, Lim JS, Hong HS, Chung YE, Choi JY. Added value of gadoxetic acid–enhanced hepatobiliary phase MR imaging in the diagnosis of hepatocellular carcinoma. Radiology 2010;255(2):459–466.
34. Golfieri R, Renzulli M, Lucidi V, Corcioni B, Trevisani F, Bolondi L. Contribution of the hepatobiliary phase of Gd-EOB-DTPA-enhanced MRI to dynamic MRI in the detection of hypovascular small (□ 2 cm) HCC in cirrhosis. Eur Radiol 2011;21(6):1233–1242.
35. Sano K, Ichikawa T, Motosugi U, et al. Imaging study of early hepatocellular carcinoma: usefulness of gadoxetic acid–enhanced MR imaging. Radiology 2011;261(3): 834–844.
36. Haradome H, Grazioli L, Tinti R, et al. Additional value of gadoxetic acid-DTPA-enhanced hepatobiliary phase MR imaging in the diagnosis of early-stage hepatocellular carcinoma: comparison with dynamic triple-phase multi- detector CT imaging. J Magn Reson Imaging 2011;34(1): 69–78.
37. Orlacchio A, Chegai F, Fabiano S, et al. Role of MRI with hepatospecific contrast agent in the identification and characterization of focal liver lesions: pathological correlation in explanted livers. Radiol Med (Torino) 2016;121(7):588–596.
38. Lee MH, Kim SH, Park MJ, Park CK, Rhim H. Gadoxetic acid-enhanced hepatobiliary phase MRI and high-b-value diffusion-weighted imaging to distinguish well-differen- tiated hepatocellular carcinomas from benign nodules in patients with chronic liver disease. AJR Am J Roentgenol 2011;197(5):W868–W875.
39. Sun HY, Lee JM, Shin CI, et al. Gadoxetic acid-enhanced magnetic resonance imaging for differentiating small hepa- tocellular carcinomas (< or = 2 cm in diameter) from arterial enhancing pseudolesions: special emphasis on hepatobiliary phase imaging. Invest Radiol 2010;45(2):96–103.
40. Darnell A, Forner A, Rimola J, etal. Liver Imaging Reporting and Data System with MR imaging: evaluation in nodules 20 mm or smaller detected in cirrhosis at screening US. Radiology 2015;275(3):698–707.
41. Chou R, Cuevas C, Fu R, et al. Imaging techniques for the diagnosis of hepatocellular carcinoma: a systematic review and meta-analysis. Ann Intern Med 2015;162(10): 697–711.
42. Tezuka M, Hayashi K, Kubota K, et al. Growth rate of lo- cally recurrent hepatocellular carcinoma after transcatheter

arterial chemoembolization: comparing the growth rate of locally recurrent tumor with that of primary hepatocellular carcinoma. Dig Dis Sci 2007;52(3):783–788.
43. Kim H, Park MS, Choi JY, et al. Can microvessel invasion of hepatocellular carcinoma be predicted by pre-operative MRI? Eur Radiol 2009;19(7):1744–1751.
44. Nishie A, Yoshimitsu K, Asayama Y, et al. Radiologic detect- ability of minute portal venous invasion in hepatocellular carcinoma. AJR Am J Roentgenol 2008;190(1):81–87.
45. Ueda K, Matsui O, Kawamori Y, et al. Hypervascular hepatocellular carcinoma: evaluation of hemodynamics with dynamic CT during hepatic arteriography. Radiology 1998;206(1):161–166.
46. Kitao A, Zen Y, Matsui O, et al. Hepatocellular carcinoma: signal intensity at gadoxetic acid–enhanced MR imaging— correlation with molecular transporters and histopathologic features. Radiology 2010;256(3):817–826.
47. Matsui O, Kobayashi S, Sanada J, et al. Hepatocelluar nodules in liver cirrhosis: hemodynamic evaluation (angiography-assisted CT) with special reference to multi-step hepatocarcinogenesis. Abdom Imaging 2011;36 (3):264–272.
48. Miyayama S, Yamashiro M, Okuda M, et al. Detection of corona enhancement of hypervascular hepatocellular carci- noma by C-arm dual-phase cone-beam CT during hepatic arteriography. Cardiovasc Intervent Radiol 2011;34(1): 81–86.
49. Ahn SY, Lee JM, Joo I, et al. Prediction of microvascular invasion of hepatocellular carcinoma using gadoxetic acid- enhanced MR and (18)F-FDG PET/CT. Abdom Imaging 2015;40(4):843–851.
50. Sakon M, Nagano H, Nakamori S, et al. Intrahepatic recurrences of hepatocellular carcinoma after hepatec- tomy: analysis based on tumor hemodynamics. Arch Surg 2002;137(1):94–99.
51. Semelka RC, Hussain SM, Marcos HB, Woosley JT. Peri- lesional enhancement of hepatic metastases: correlation between MR imaging and histopathologic findings— initial observations. Radiology 2000;215(1):89–94.
52. Ito K, Fujita T, Shimizu A, et al. Multiarterial phase dynamic MRI of small early enhancing hepatic lesions in cirrhosis or chronic hepatitis: differentiating between hypervascular hepatocellular carcinomas and pseudolesions. AJR Am J Roentgenol 2004;183(3):699–705.
53. Choi JY, Lee JM, Sirlin CB. CT and MR imaging diagnosis and staging of hepatocellular carcinoma. II. Extracellular agents, hepatobiliary agents, and ancillary imaging features. Radiology 2014;273(1):30–50.
54. Matsui O, Kadoya M, Takahashi S, et al. Focal sparing of segment IV in fatty livers shown by sonography and CT: correlation with aberrant gastric venous drainage. AJR Am J Roentgenol 1995;164(5):1137–1140.
55. Lim KS. Diffusion-weighted MRI of hepatocellular carci- noma in cirrhosis. Clin Radiol 2014;69(1):1–10.
56. Taouli B, Vilgrain V, Dumont E, Daire JL, Fan B, Menu Y. Evaluation of liver diffusion isotropy and characterization of focal hepatic lesions with two single-shot echo-planar MR imaging sequences: prospective study in 66 patients. Radiology 2003;226(1):71–78.
57. Taouli B, Tolia AJ, Losada M, et al. Diffusion-weighted MRI for quantification of liver fibrosis: preliminary experi- ence. AJR Am J Roentgenol 2007;189(4):799–806.
58. Kim AY, Kim YK, Lee MW, et al. Detection of hepato- cellular carcinoma in gadoxetic acid-enhanced MRI and diffusion-weighted MRI with respect to the severity of liver cirrhosis. Acta Radiol 2012;53(8):830–838.
59. Kim YK, Lee WJ, Park MJ, Kim SH, Rhim H, Choi D. Hypovascular hypointense nodules on hepatobiliary phase gadoxetic acid–enhanced MR images in patients with cirrhosis: potential of DW imaging in predicting pro- gression to hypervascular HCC. Radiology 2012;265(1): 104–114.
60. Catalano OA, Choy G, Zhu A, Hahn PF, Sahani DV. Dif- ferentiation of malignant thrombus from bland thrombus of the portal vein in patients with hepatocellular carcinoma: application of diffusion-weighted MR imaging. Radiology 2010;254(1):154–162.

61. Nishie A, Tajima T, Asayama Y, et al. Diagnostic per- formance of apparent diffusion coefficient for predicting histological grade of hepatocellular carcinoma. Eur J Radiol 2011;80(2):e29–e33.
62. Le Moigne F, Boussel L, Haquin A, et al. Grading of small hepatocellular carcinomas (≤2 cm): correlation between histology, T2 and diffusion-weighted imaging. Br J Radiol 2014;87(1041):20130763.
63. Guiu B, Cercueil JP. Liver diffusion-weighted MR imaging: the tower of Babel? Eur Radiol 2011;21(3):463–467.
64. Piana G, Trinquart L, Meskine N, Barrau V, Beers BV, Vil- grain V. New MR imaging criteria with a diffusion-weighted sequence for the diagnosis of hepatocellular carcinoma in chronic liver diseases. J Hepatol 2011;55(1):126–132.
65. Kadoya M, Matsui O, Takashima T, Nonomura A. Hepatocellular carcinoma: correlation of MR imaging and histopathologic findings. Radiology 1992;183(3): 819–825.
66. Ohtomo K, Baron RL, Dodd GD 3rd, Federle MP, Ohtomo Y, Confer SR. Confluent hepatic fibrosis in advanced cir- rhosis: evaluation with MR imaging. Radiology 1993;189(3):871–874.
67. Matsui O, Kadoya M, Kameyama T, et al. Adenomatous hyperplastic nodules in the cirrhotic liver: differentiation from hepatocellular carcinoma with MR imaging. Radiology 1989;173(1):123–126.
68. Earls JP, Theise ND, Weinreb JC, et al. Dysplastic nodules and hepatocellular carcinoma: thin-section MR imaging of explanted cirrhotic livers with pathologic correlation. Radiology 1996;201(1):207–214.
69. Krinsky GA, Lee VS. MR imaging of cirrhotic nodules. Abdom Imaging 2000;25(5):471–482.
70. Kim T, Baron RL, Nalesnik MA. Infarcted regenerative nodules in cirrhosis: CT and MR imaging findings with pathologic correlation. AJR Am J Roentgenol 2000;175(4): 1121–1125.
71. Vilgrain V, Lewin M, Vons C, et al. Hepatic nodules in Budd- Chiari syndrome: imaging features. Radiology 1999;210(2):443–450.
72. Hussain HK, Syed I, Nghiem HV, et al. T2-weighted MR imaging in the assessment of cirrhotic liver. Radiology 2004;230(3):637–644.
73. Kamura T, Kimura M, Sakai K, et al. Small hypervascular hepatocellular carcinoma versus hypervascular pseudole- sions: differential diagnosis on MRI. Abdom Imaging 2002;27(3):315–324.
74. van den Bos IC, Hussain SM, Dwarkasing RS, et al. MR imaging of hepatocellular carcinoma: relationship between lesion size and imaging findings, including signal intensity and dynamic enhancement patterns. J Magn Reson Imaging 2007;26(6):1548–1555.
75. Honda H, Kaneko K, Maeda T, et al. Small hepatocellular carcinoma on magnetic resonance imaging: relation of signal intensity to angiographic and clinicopathologic findings. Invest Radiol 1997;32(3):161–168.
76. Jha RC, Zanello PA, Nguyen XM, et al. Small hepatocel- lular carcinoma: MRI findings for predicting tumor growth rates. Acad Radiol 2014;21(11):1455–1464.
77. Muramatsu Y, Nawano S, Takayasu K, et al. Early hepa- tocellular carcinoma: MR imaging. Radiology 1991;181(1):209–213.
78. Ebara M, Fukuda H, Kojima Y, et al. Small hepatocellular carcinoma: relationship of signal intensity to histopathologic findings and metal content of the tumor and surrounding hepatic parenchyma. Radiology 1999;210(1):81–88.
79. Enomoto S, Tamai H, Shingaki N, et al. Assessment of hepatocellular carcinomas using conventional magnetic resonance imaging correlated with histological differentia- tion and a serum marker of poor prognosis. Hepatol Int 2011;5(2):730–737.
80. Hyodo T, Murakami T, Imai Y, et al. Hypovascular nod- ules in patients with chronic liver disease: risk factors for development of hypervascular hepatocellular carcinoma. Radiology 2013;266(2):480–490.
81. Labranche R, Gilbert G, Cerny M, et al. Liver iron quan- tification with MR imaging: a primer for radiologists. RadioGraphics 2018;38(2):392–412.

82. Terada T, Nakanuma Y. Iron-negative foci in siderotic macroregenerative nodules in human cirrhotic liver: a marker of incipient neoplastic lesions. Arch Pathol Lab Med 1989;113(8):916–920.
83. Terada T, Kadoya M, Nakanuma Y, Matsui O. Iron-accu- mulating adenomatous hyperplastic nodule with malignant foci in the cirrhotic liver: histopathologic, quantitative iron, and magnetic resonance imaging in vitro studies. Cancer 1990;65(9):1994–2000.
84. Zhang J, Krinsky GA. Iron-containing nodules of cirrhosis. NMR Biomed 2004;17(7):459–464.
85. Mitchell DG, Rubin R, Siegelman ES, Burk DL Jr, Rifkin MD. Hepatocellular carcinoma within siderotic regenerative nodules: appearance as a nodule within a nodule on MR images. Radiology 1991;178(1):101–103.
86. Deugnier YM, Charalambous P, Le Quilleuc D, et al. Pre- neoplastic significance of hepatic iron-free foci in genetic hemochromatosis: a study of 185 patients. Hepatology 1993;18(6):1363–1369.
87. Guyader D, Gandon Y, Sapey T, et al. Magnetic resonance iron-free nodules in genetic hemochromatosis. Am J Gas- troenterol 1999;94(4):1083–1086.
88. Nakamura Y, Toyota N, Date S, et al. Clinical signifi- cance of the transitional phase at gadoxetate disodium- enhanced hepatic MRI for the diagnosis of hepatocellular carcinoma: preliminary results. J Comput Assist Tomogr 2011;35(6):723–727.
89. Ringe KI, Husarik DB, Sirlin CB, Merkle EM. Gadoxetate disodium-enhanced MRI of the liver. I. Protocol optimiza- tion and lesion appearance in the noncirrhotic liver. AJR Am J Roentgenol 2010;195(1):13–28.
90. Narita M, Hatano E, Arizono S, et al. Expression of OATP1B3 determines uptake of Gd-EOB-DTPA in hepatocellular carcinoma. J Gastroenterol 2009;44(7): 793–798.
91. Rhee H, Kim MJ, Park YN, Choi JS, Kim KS. Gadoxetic acid-enhanced MRI findings of early hepatocellular carci- noma as defined by new histologic criteria. J Magn Reson Imaging 2012;35(2):393–398.
92. Bartolozzi C, Battaglia V, Bargellini I, et al. Contrast- enhanced magnetic resonance imaging of 102 nodules in cirrhosis: correlation with histological findings on explanted livers. Abdom Imaging 2013;38(2): 290–296.
93. Cortis K, Liotta R, Miraglia R, Caruso S, Tuzzolino F, Luca A. Incorporating the hepatobiliary phase of gado- benate dimeglumine-enhanced MRI in the diagnosis of hepatocellular carcinoma: increasing the sensitivity with- out compromising specificity. Acta Radiol 2016;57(8): 923–931.
94. Chen N, Motosugi U, Morisaka H, et al. Added value of a gadoxetic acid-enhanced hepatocyte-phase image to the LI-RADS system for diagnosing hepatocellular carcinoma. Magn Reson Med Sci 2016;15(1):49–59.
95. Kogita S, Imai Y, Okada M, et al. Gd-EOB-DTPA-enhanced magnetic resonance images of hepatocellular carcinoma: correlation with histological grading and portal blood flow. Eur Radiol 2010;20(10):2405–2413.
96. Kim KA, Kim MJ, Jeon HM, et al. Prediction of micro- vascular invasion of hepatocellular carcinoma: usefulness of peritumoral hypointensity seen on gadoxetate disodium- enhanced hepatobiliary phase images. J Magn Reson Imaging 2012;35(3):629–634.
97. Horvat N, Nikolovski I, Long N, et al. Imaging features of hepatocellular carcinoma compared to intrahepatic chol- angiocarcinoma and combined tumor on MRI using liver imaging and data system (LI-RADS) version 2014. Abdom Radiol (NY) 2018;43(1):169–178.
98. Bae JS, Kim JH, Yu MH, et al. Diagnostic accuracy of gadoxetic acid-enhanced MR for small hypervascular he- patocellular carcinoma and the concordance rate of Liver Imaging Reporting and Data System (LI-RADS). PLoS One 2017;12(5):e0178495.
99. Stevens WR, Gulino SP, Batts KP, Stephens DH, Johnson CD. Mosaic pattern of hepatocellular carcinoma: histologic basis for a characteristic CT appearance. J Comput Assist Tomogr 1996;20(3):337–342.

100. Choi BI, Takayasu K, Han MC. Small hepatocellular carci- nomas and associated nodular lesions of the liver: pathology, pathogenesis, and imaging findings. AJR Am J Roentgenol 1993;160(6):1177–1187.
101. Kojiro M. 'Nodule-in-nodule' appearance in hepato- cellular carcinoma: its significance as a morphologic marker of dedifferentiation. Intervirology 2004;47(3-5):179–183.
102. Efremidis SC, Hytiroglou P. The multistep process of hepatocarcinogenesis in cirrhosis with imaging correlation. Eur Radiol 2002;12(4):753–764.
103. Ueda K, Terada T, Nakanuma Y, Matsui O. Vascular supply in adenomatous hyperplasia of the liver and hepa- tocellular carcinoma: a morphometric study. Hum Pathol 1992;23(6):619–626.
104. Efremidis SC, Hytiroglou P, Matsui O. Enhancement pat- terns and signal-intensity characteristics of small hepatocel- lular carcinoma in cirrhosis: pathologic basis and diagnostic challenges. Eur Radiol 2007;17(11):2969–2982.
105. Hanna RF, Aguirre DA, Kased N, Emery SC, Peterson MR, Sirlin CB. Cirrhosis-associated hepatocellular nodules: correlation of histopathologic and MR imaging features. RadioGraphics 2008;28(3):747–769.
106. Sadek AG, Mitchell DG, Siegelman ES, Outwater EK, Matteuccí T, Hann HW. Early hepatocellular carcinoma that develops within macroregenerative nodules: growth rate depicted at serial MR imaging. Radiology 1995;195(3):753–756.
107. Kojiro M, Roskams T. Early hepatocellular carcinoma and dysplastic nodules. Semin Liver Dis 2005;25(2): 133–142.
108. Cruite I, Santillan C, Mamidipalli A, Shah A, Tang A, Sirlin CB. Liver Imaging Reporting and Data System: review of ancillary imaging features. Semin Roentgenol 2016;51(4):301–307.
109. Yu JS, Chung JJ, Kim JH, Kim KW. Fat-containing nod- ules in the cirrhotic liver: chemical shift MRI features and clinical implications. AJR Am J Roentgenol 2007;188(4):1009–1016.
110. Park HJ, Jang KM, Kang TW, et al. Identification of imaging predictors discriminating different primary liver tumours in patients with chronic liver disease on gadoxetic acid-enhanced MRI: a classification tree analysis. Eur Radiol 2016;26(9):3102–3111.
111. Seymour K, Charnley RM. Evidence that metastasis is less common in cirrhotic than normal liver: a systematic review of post-mortem case-control studies. Br J Surg 1999;86(10):1237–1242.
112. Kim TK, Lee KH, Jang HJ, et al. Analysis of gadobenate dimeglumine–enhanced MR findings for characterizing small (1–2-cm) hepatic nodules in patients at high risk for hepatocellular carcinoma. Radiology 2011;259(3): 730–738.
113. Rimola J, Forner A, Tremosini S, et al. Non-invasive diagnosis of hepatocellular carcinoma □ 2 cm in cirrhosis: diagnostic accuracy assessing fat, capsule and signal intensity at dynamic MRI. J Hepatol 2012;56(6):1317–1323.
114. Sheng RF, Zeng MS, Ji Y, Yang L, Chen CZ, Rao SX. MR features of small hepatocellular carcinoma in normal, fibrotic, and cirrhotic livers: a comparative study. Abdom Imaging 2015;40(8):3062–3069.
115. Casillas VJ, Amendola MA, Gascue A, Pinnar N, Levi JU, Perez JM. Imaging of nontraumatic hemorrhagic hepatic lesions. RadioGraphics 2000;20(2):367–378.
116. Whitney WS, Herfkens RJ, Jeffrey RB, et al. Dynamic breath-hold multiplanar spoiled gradient-recalled MR imaging with gadolinium enhancement for differentiating hepatic hemangiomas from malignancies at 1.5 T. Radiology 1993;189(3):863–870.
117. Motosugi U, Ichikawa T, Onohara K, et al. Distinguishing hepatic metastasis from hemangioma using gadoxetic acid- enhanced magnetic resonance imaging. Invest Radiol 2011;46(6):359–365.
118. Taouli B, Goh JS, Lu Y, et al. Growth rate of hepatocellular carcinoma: evaluation with serial computed tomography or magnetic resonance imaging. J Comput Assist Tomogr 2005;29(4):425–429.

119. De Rose AM, Cucchetti A, Clemente G, et al. Prognostic significance of tumor doubling time in mass-forming type cholangiocarcinoma. J Gastrointest Surg 2013;17(4):739–747.
120. Oquiñena S, Iñarrairaegui M, Vila JJ, Alegre F, Zozaya JM, Sangro B. Spontaneous regression of hepatocellular carcinoma: three case reports and a categorized review of the literature. Dig Dis Sci 2009;54(5):1147–1153.
121. Huz JI, Melis M, Sarpel U. Spontaneous regression of hepatocellular carcinoma is most often associated with tumour hypoxia or a systemic inflammatory response. HPB 2012;14(8):500–505.
122. Brancatelli G, Federle MP, Blachar A, Grazioli L. Heman- gioma in the cirrhotic liver: diagnosis and natural history. Radiology 2001;219(1):69–74.
123. Semelka RC, Brown ED, Ascher SM, et al. Hepatic hem- angiomas: a multi-institutional study of appearance on T2-weighted and serial gadolinium-enhanced gradient-echo MR images. Radiology 1994;192(2):401–406.
124. Tamada T, Ito K, Yamamoto A, et al. Hepatic hemangiomas: evaluation of enhancement patterns at dynamic MRI with gadoxetate disodium. AJR Am J Roentgenol 2011;196(4):824–830.
125. Brancatelli G, Baron RL, Peterson MS, Marsh W. Helical CT screening for hepatocellular carcinoma in patients with cirrhosis: frequency and causes of false-positive interpreta- tion. AJR Am J Roentgenol 2003;180(4):1007–1014.
126. Krinsky GA, Lee VS, Theise ND, et al. Hepatocellular carcinoma and dysplastic nodules in patients with cirrhosis: prospective diagnosis with MR imaging and explantation correlation. Radiology 2001;219(2):445–454.
127. Mortelé KJ, Ros PR. Cystic focal liver lesions in the adult: differential CT and MR imaging features. RadioGraphics 2001;21(4):895–910.
128. Ahn SJ, Kim MJ, Hong HS, Kim KA, Song HT. Distinguish- ing hemangiomas from malignant solid hepatic lesions: a comparison of heavily T2-weighted images obtained before and after administration of gadoxetic acid. J Magn Reson Imaging 2011;34(2):310–317.
129. Cruite I, Schroeder M, Merkle EM, Sirlin CB. Gadoxetate disodium-enhanced MRI of the liver. II. Protocol optimiza- tion and lesion appearance in the cirrhotic liver. AJR Am J Roentgenol 2010;195(1):29–41.
130. Hope TA, Fowler KJ, Sirlin CB, et al. Hepatobiliary agents and their role in LI-RADS. Abdom Imaging 2015;40(3):613–625.
131. Park Y, Kim SH, Kim SH, et al. Gadoxetic acid (Gd-EOB- DTPA)-enhanced MRI versus gadobenate dimeglumine (Gd-BOPTA)-enhanced MRI for preoperatively detecting hepatocellular carcinoma: an initial experience. Korean J Radiol 2010;11(4):433–440.
132. Choi JW, Lee JM, Kim SJ, et al. Hepatocellular carcinoma: imaging patterns on gadoxetic acid–enhanced MR im- ages and their value as an imaging biomarker. Radiology 2013;267(3):776–786.

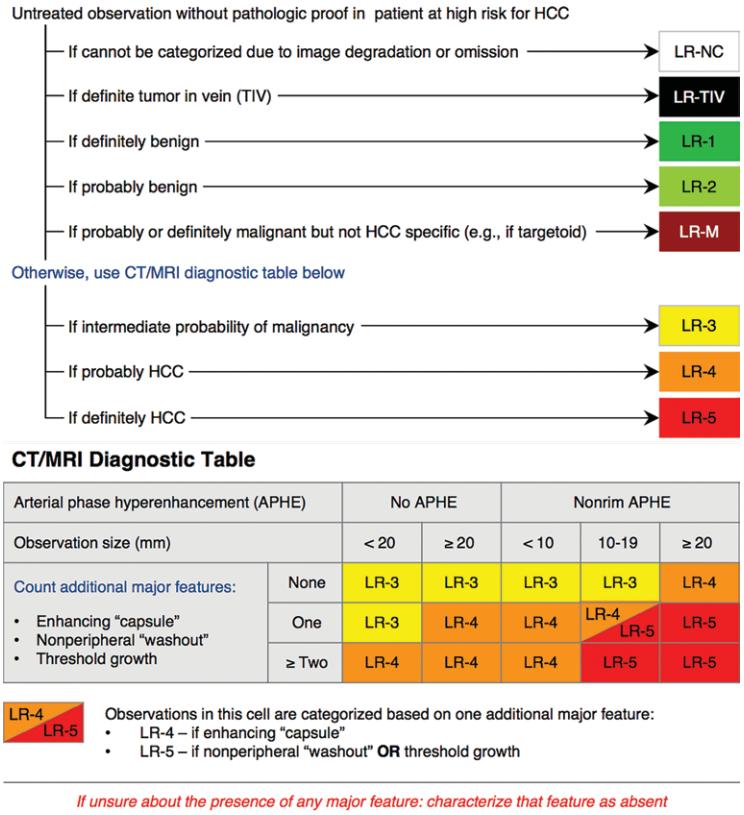

Figure 1. LI-RADS diagnostic algorithm and table. *APHE* = arterial phase hyperenhancement.

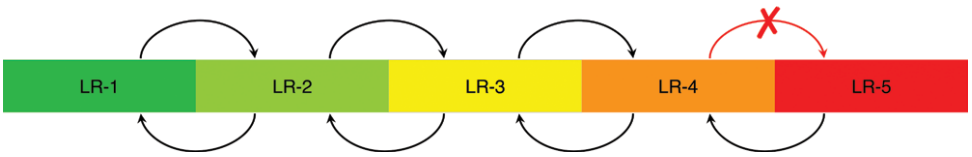

Figure 2. Rules for application of ancillary features. Use of ancillary features is optional. Ancillary features that favor malignancy in general or HCC in particular may be used to upgrade by one category only and may not be used to upgrade from LR-4 to LR-5. Ancillary features that favor benignity may be used to downgrade by one category.

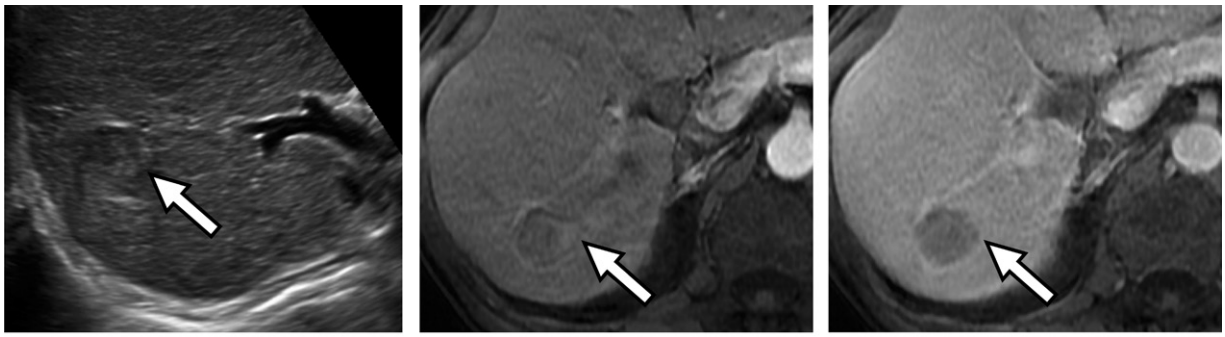

Figure 3. US visibility of HCC as a discrete nodule or mass in a 67-year-old man with chronic hepatitis B infection. (a) On a non- enhanced screening US image, an MRI-detected observation is visible as a discrete nodule or mass (arrow). (b, c) Axial T1-weighted fat-saturated images in the late arterial (b) and portal venous (c) phases show the corresponding MRI-detected observation (arrow). Pathologic analysis of the hepatectomy specimen demonstrated HCC.

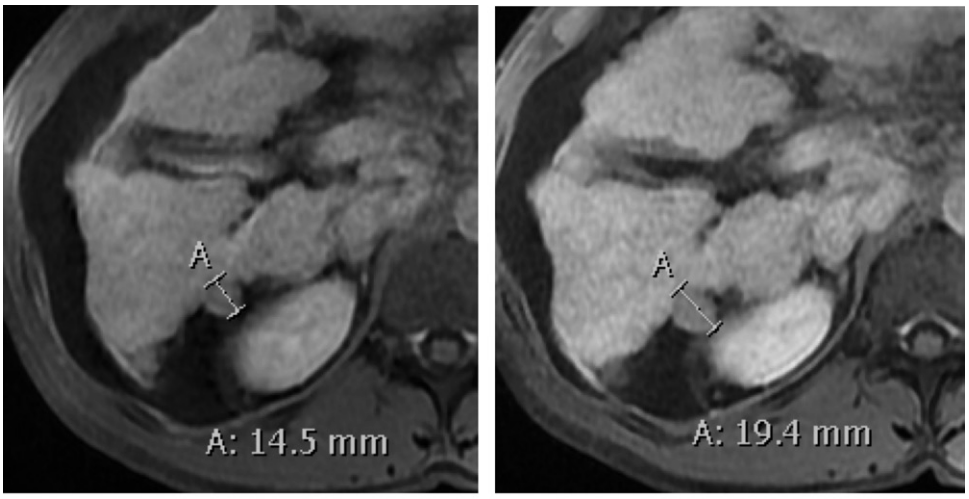

a. b.

Figure 4. Subthreshold growth of a distinctive nodule in a 37-year-old man with autoimmune cirrhosis. Baseline delayed phase image (a) and follow-up image 6 months later (b) show subthreshold growth (see measurements). Pathologic analysis of the liver specimen demonstrated HCC.

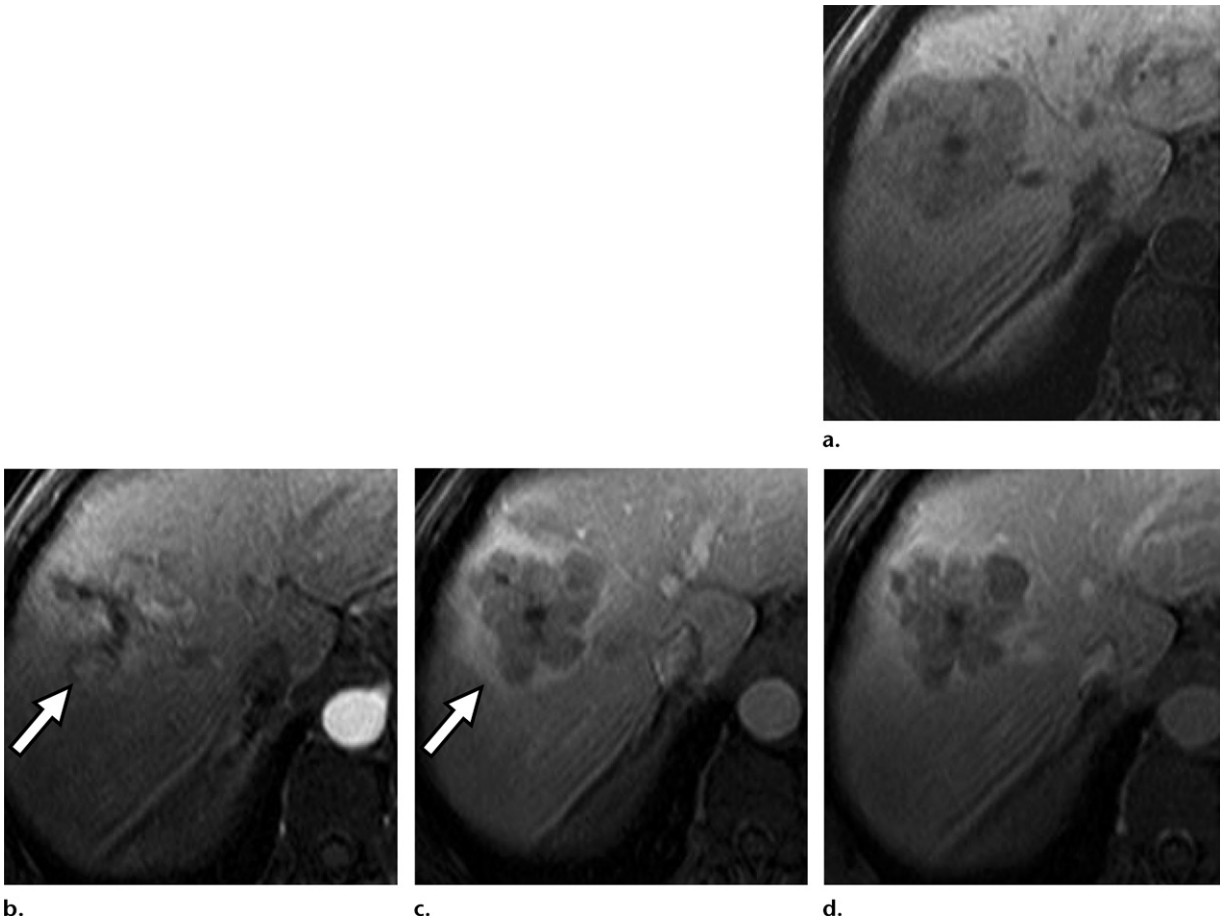

Figure 5. Corona enhancement of HCC in a 61-year-old man with hepatitis C infec- tion. Axial T1-weighted fat-saturated images obtained before contrast material administration (a) and in the late arterial (b), portal venous (c), and delayed (d) phases show corona enhancement (arrow in b and c).

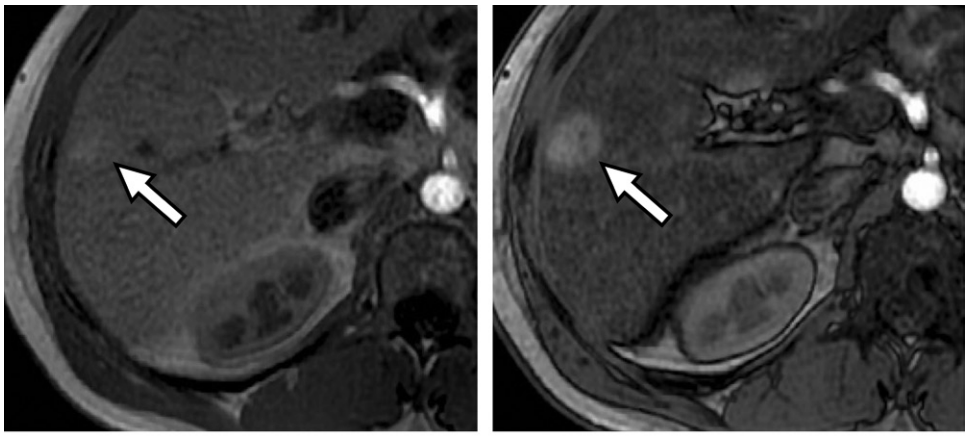

a. b.

Figure 6. Fat sparing in a solid mass (a dysplastic nodule) in a 41-year-old man under surveillance for cryptogenic cirrhosis. Axial in-phase (a) and out-of- phase (b) T1-weighted images show fat sparing in a solid mass (arrow), in contrast to the signal drop of the background liver seen on the out-of- phase image. Biopsy of the mass demonstrated high-grade dysplasia.

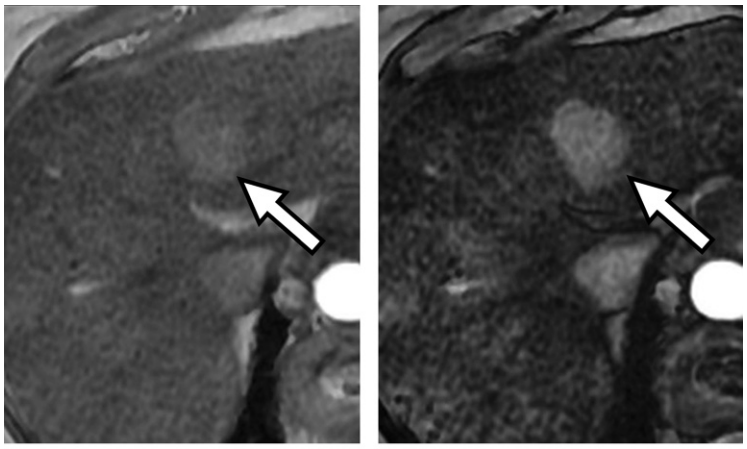

Figure 7. Fat sparing in a solid mass (HCC) in a 75-year-old woman with hepatitis C infection. Axial in-phase (echo time [TE] = 4.6 msec) **(a)** and out-of-phase (TE = 2.3 msec) **(b)** T1-weighted images show fat sparing in a solid mass (arrow), in contrast to the signal drop in the background liver on the out-of-phase image.

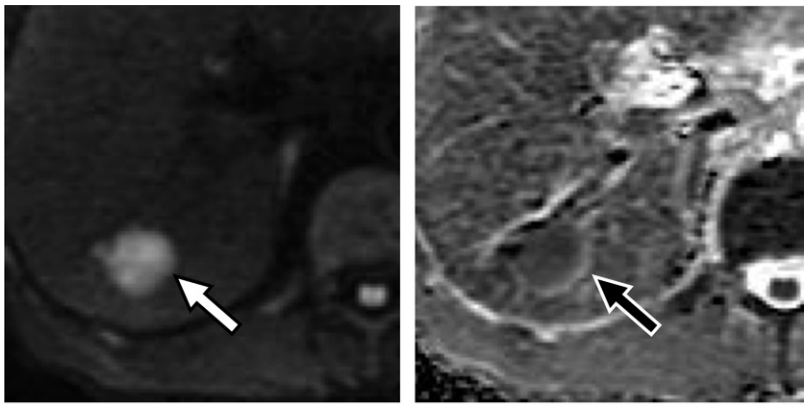

a. b.

Figure 8. Restricted diffusion in HCC in a 67-year-old man under surveillance for chronic hepatitis B with human im- munodeficiency virus (HIV) coinfection. Axial diffusion-weighted image (b = 800 sec/mm2) (a) and ADC map (b) show restricted diffusion (arrow), appearing as high signal intensity in a and low signal intensity in b. Restricted diffusion favors malignancy in general. Pathologic analy- sis of the hepatectomy specimen demon- strated HCC.

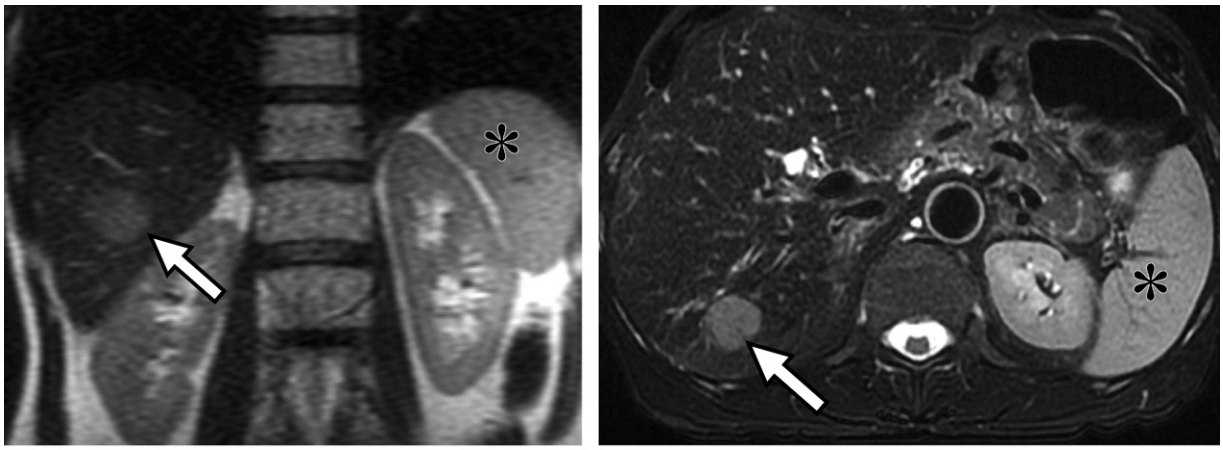

a. b.

Figure 9. Mild-moderate T2 hyperintensity of HCC in a 67-year-old man with chronic hepatitis B infection. Coronal (a) and axial (b) T2-weighted fat-saturated images show mild-moderate T2 hyperintensity (arrow), which is isointense to the spleen parenchyma (*). Pathologic analysis of the hepatectomy specimen demonstrated HCC.

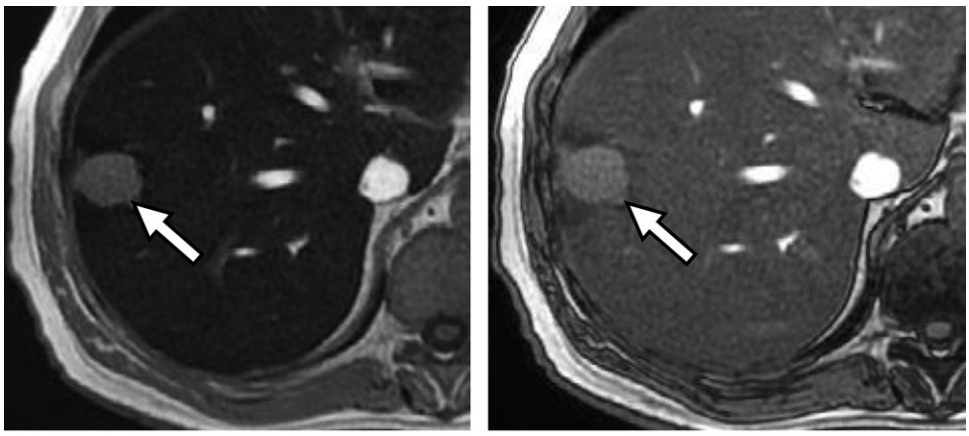

Figure 10. Iron sparing in a solid mass (cholangiocarcinoma) in a 62-year-old man with hemochromato- sis. Axial in-phase (TE = 4.6 msec) (a) and out-of-phase (TE = 2.3 msec) (b) T1-weighted images show iron sparing in a solid mass (arrow), in contrast to the signal drop in the background liver on the in-phase image, obtained with a longer TE. Pathologic analysis of the biopsy specimen demonstrated cholangiocarcinoma.

Figures 11, 12. (11) Transitional phase hypointensity of cholangiocarci- noma in a 58-year-old woman. Axial T1-weighted fat-saturated images be- fore (a) and after (b–d) administration of gadoxetate disodium in the late arterial (b), transitional (c), and hepatobiliary (d) phases show transitional phase hypointensity (arrow in c). (12) Transitional phase hypointensity of HCC in a 75-year-old woman with hepatitis C infection. Axial T1-weighted fat-saturated images before (a) and after (b–f) administration of gadoxetate disodium in the early arterial (b, c), portal venous (d), transitional (e), and hepatobiliary (f) phases show transitional phase hypointensity (arrow in e).

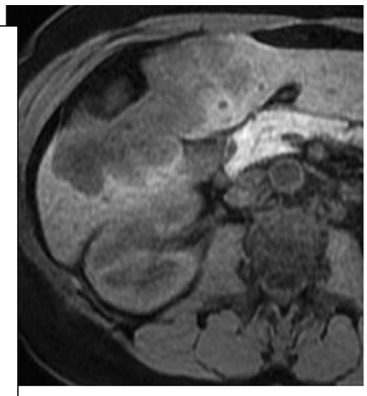

11a.

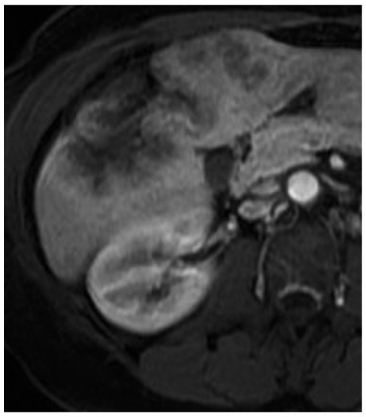

11b.

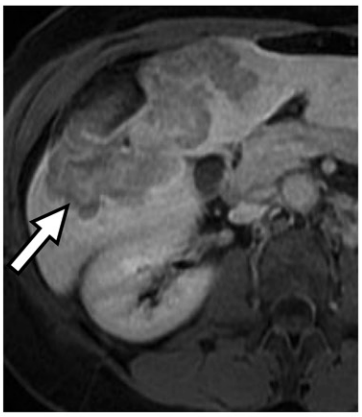

11c.

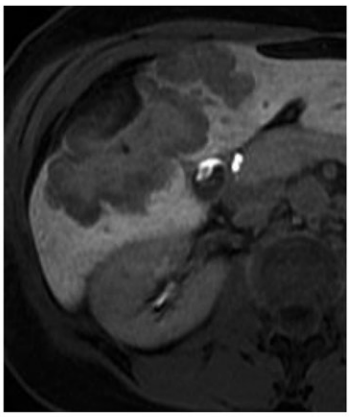

11d.

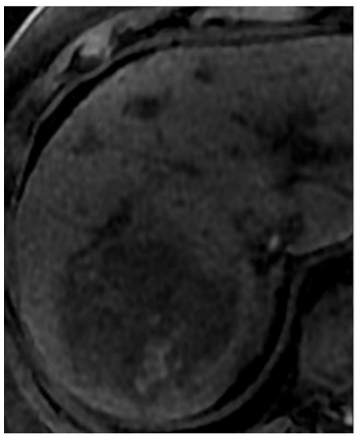

12a.

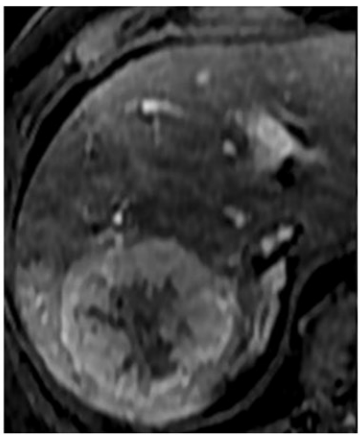

12b.

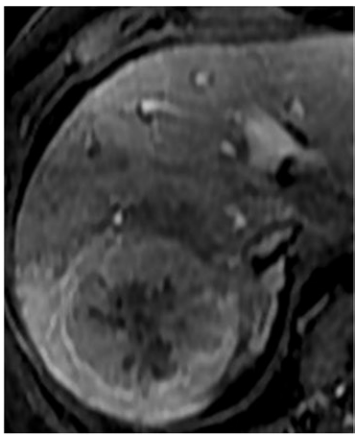

12c.

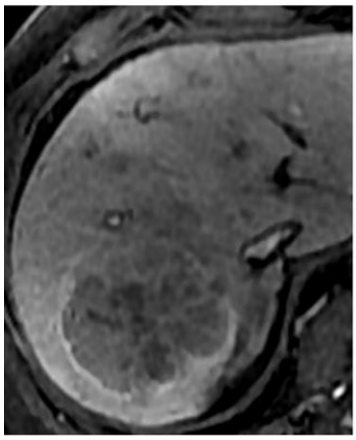

12d.

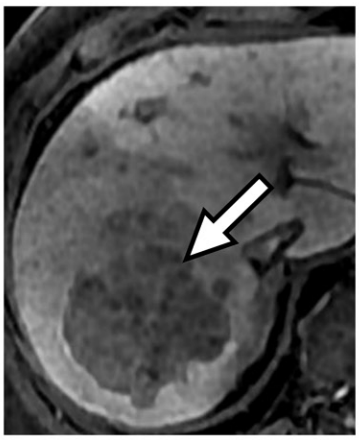

12e.

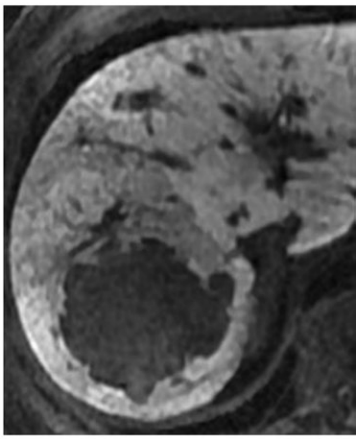

12f.

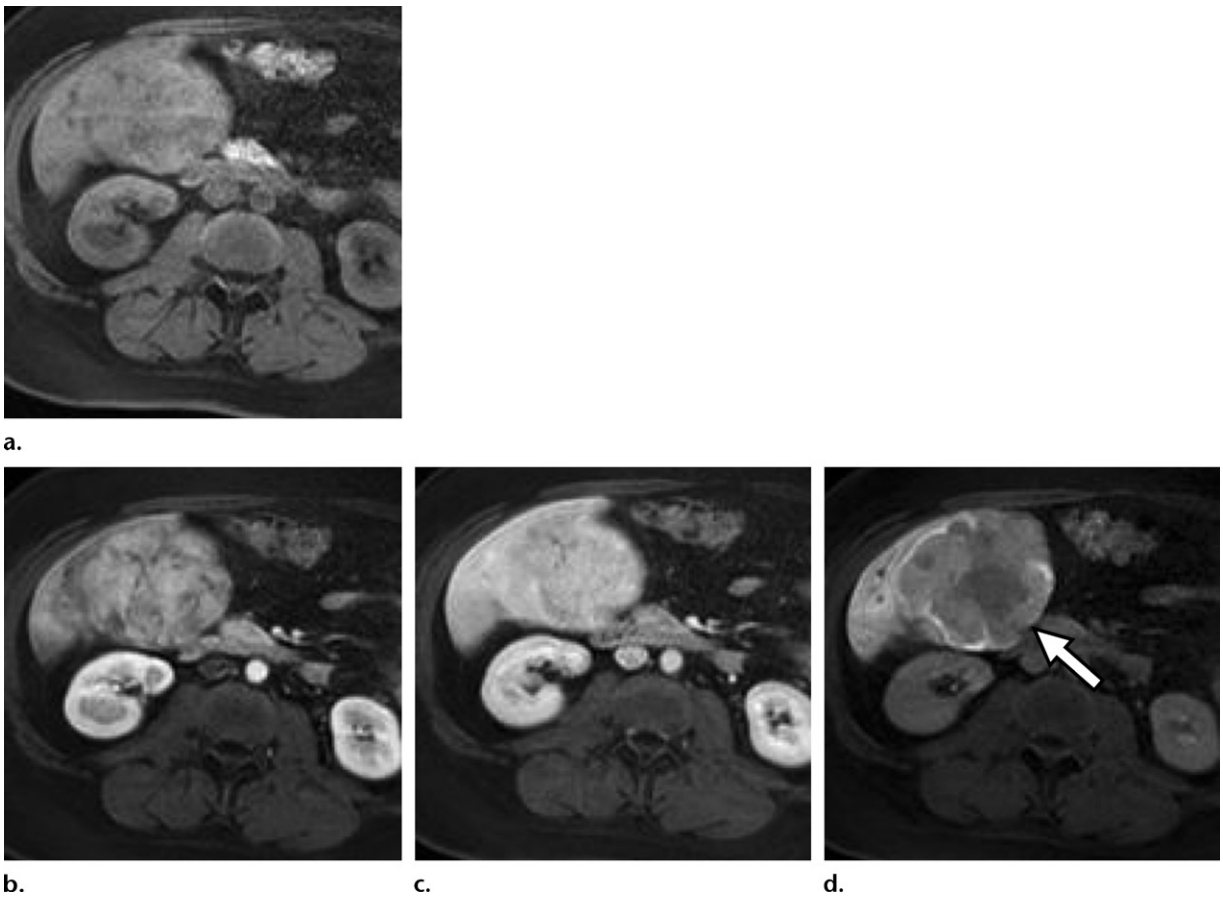

Figure 13. HBP hypointensity of HCC in a 34-year-old woman with nonalcoholic fatty liver disease. Axial T1-weighted fat-saturated images before (a) and after (b–d) administration of gadoxetate disodium in the late arterial (b), portal venous (c), and hepatobiliary (d) phases show HBP hypointensity (arrow in d). Pathologic analysis demonstrated HCC.

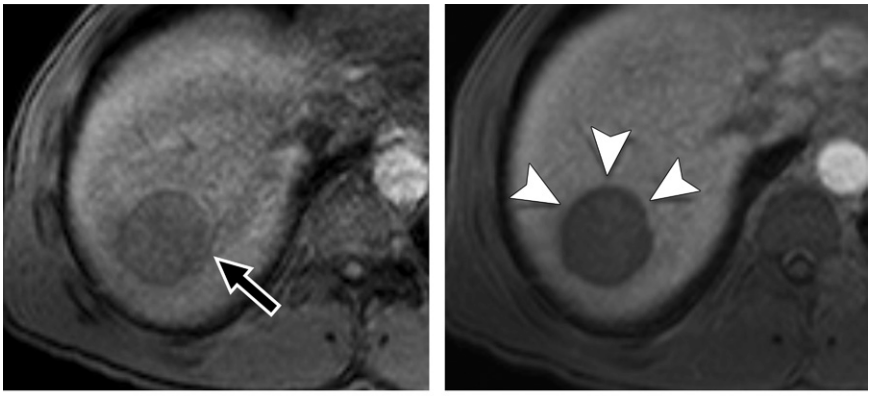

Figure 14. Nonenhancing “capsule” of HCC in a 47-year-old man with chronic hepatitis B infection. Axial T1-weighted fat-saturated images before contrast material administration **(a)** and in the HBP **(b)** show a mass (arrow in **a**) with a hypointense rim in the HBP (arrowheads in **b**), which represents a subtype of nonenhancing “capsule.”

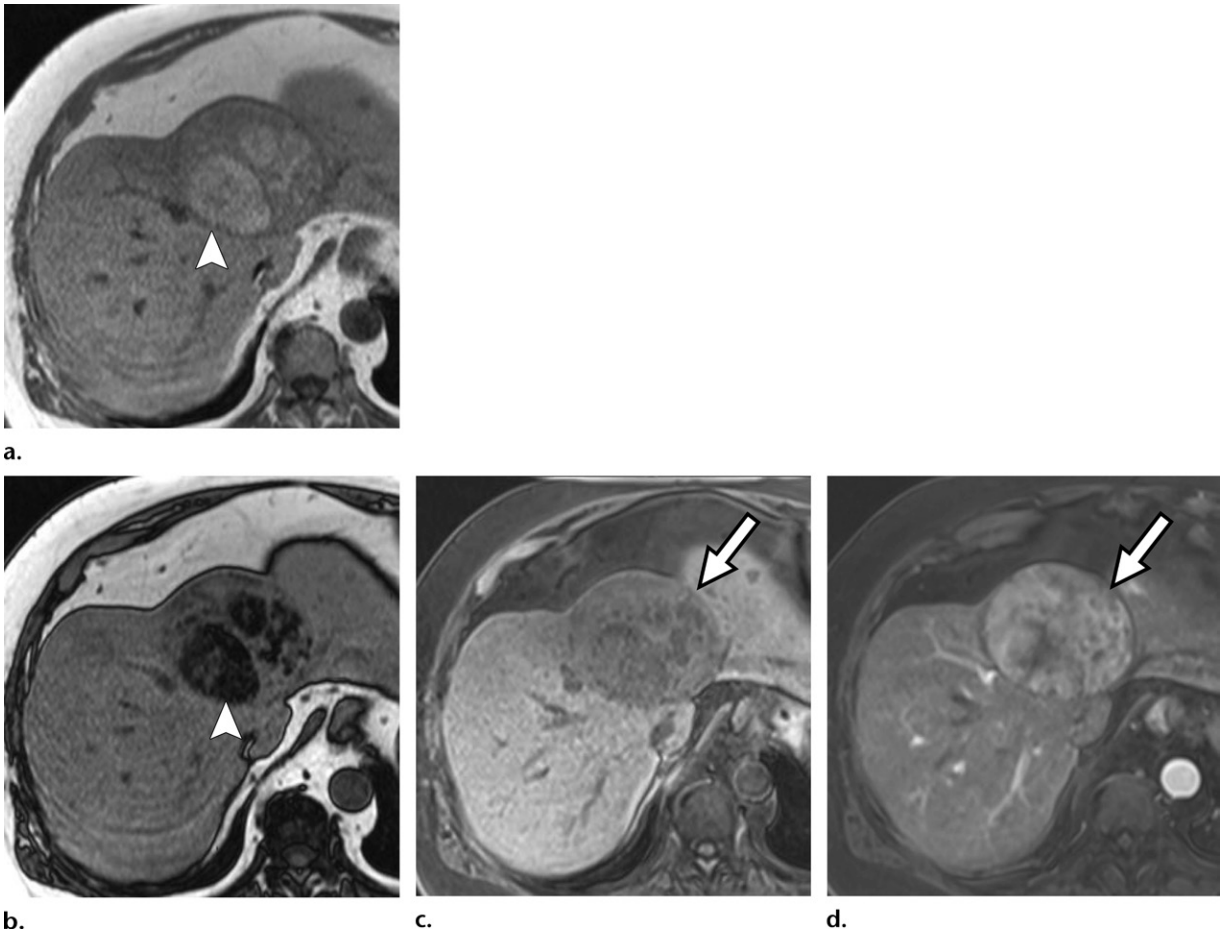

Figure 15. Mosaic architecture of HCC in a 68-year-old man with cirrhosis due to non-alcoholic steatohepatitis (NASH). Axial T1-weighted in-phase **(a)** and out-of-phase **(b)** images, axial T1-weighted fat-saturated image before contrast material administra- tion **(c)**, and corresponding image in the late arterial phase **(d)** show a heteroge- neous mass with mosaic architecture, characterized by compartments with different signal intensity characteristics, some of which contain fat (arrowhead in **a** and **b**) or demonstrate APHE (arrow in **c** and **d**). Mosaic architecture favors HCC in particular. Pathologic analysis of the hepatectomy specimen demonstrated HCC.

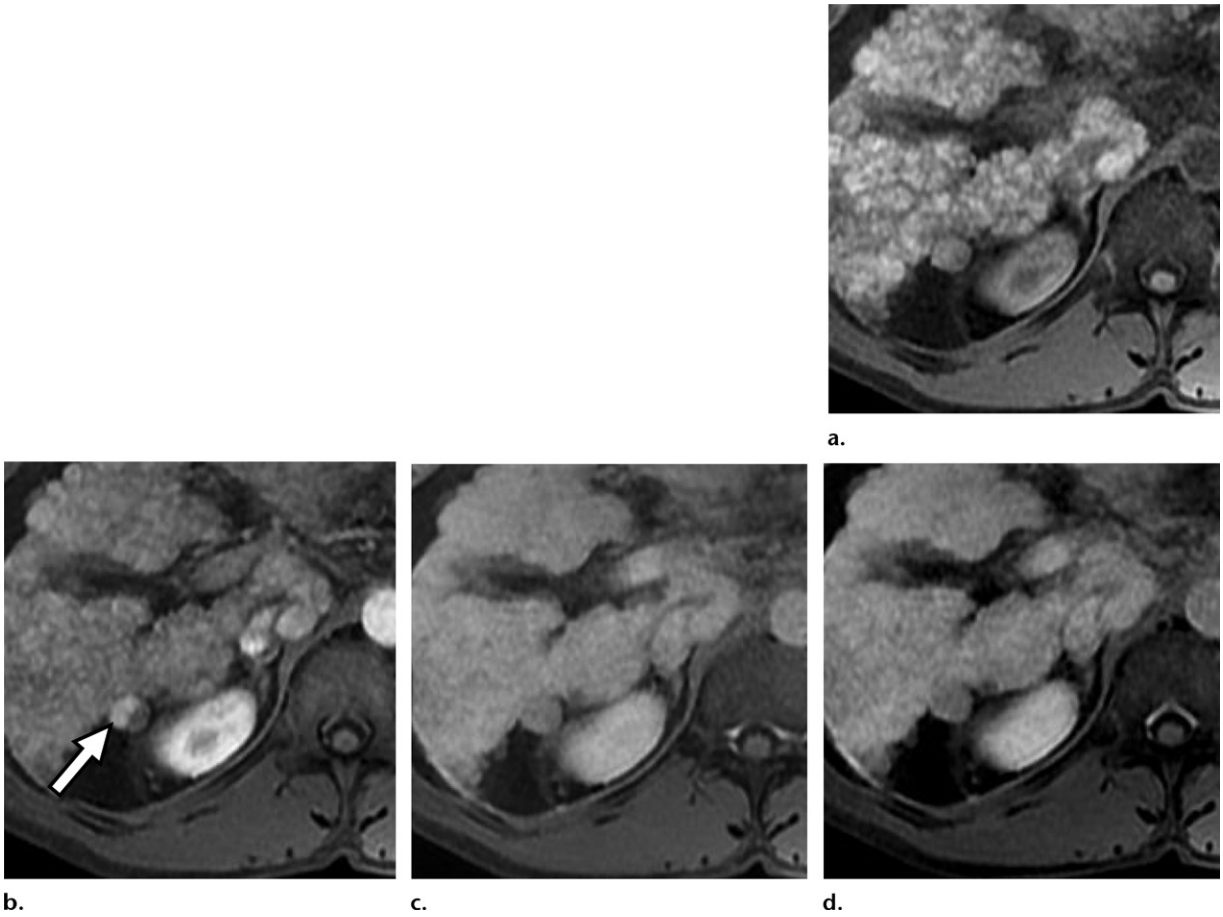

Figure 16. Nodule-in-nodule architecture of HCC in a 37-year-old man with autoimmune cirrhosis. Axial T1-weighted fat-saturated images before **(a)** and after **(b–d)** contrast material administration in the late arterial **(b)**, portal venous **(c)**, and delayed **(d)** phases show a mass with APHE of a smaller inner nodule (arow in **b**) within a larger nodule with washout. Pathologic analysis of the liver specimen demonstrated HCC.

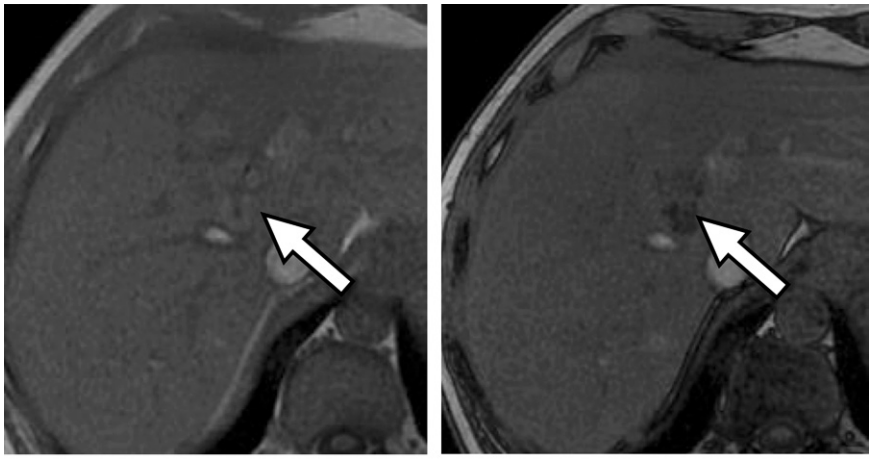

a. b.

Figure 17. Fat in a mass (HCC), more than in adjacent liver, in a 58-year-old man with hepatitis C infection. Axial in-phase **(a)** and out-of-phase **(b)** T1-weighted im- ages show a mass (arrow) with signal drop on the out-of-phase image, indicating the presence of intralesion fat. Biopsy of the mass demonstrated HCC.

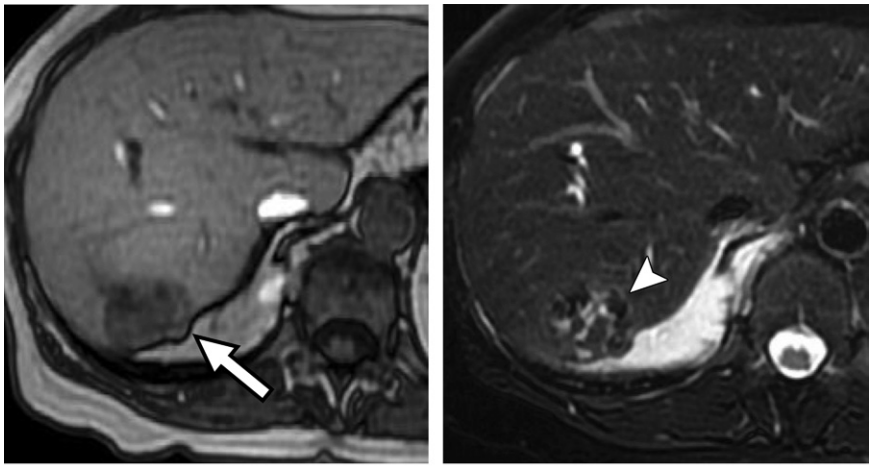

a. b.

Figure 18. Blood products in a mass in a 54-year-old man without cirrhosis documented in clinical and imaging records. (a) Axial out-of-phase T1- weighted image shows an isoin- tense right liver lobe mass (ar- row). **(b)** Axial T2-weighted fat- saturated image shows hetero- geneous blood products in the mass (arrowhead). In a high-risk patient, blood products in a mass favor the diagnosis of HCC.

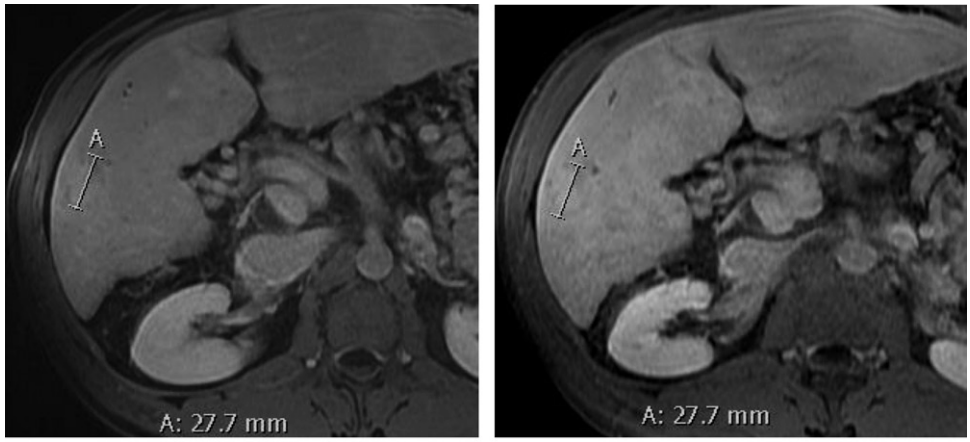

a. b.

Figure 19. Size stability for 2 years or longer of a dysplastic nodule in a 31-year-old woman undergoing surveillance for primary sclerosing cholangitis. (a) Baseline delayed phase image shows mild delayed phase hyperenhancement without washout appearance. (b) Corresponding image 3 years later shows size stabil- ity of the mass (see measurements). Biopsy of the mass demonstrated a hypervascular dysplastic nodule.

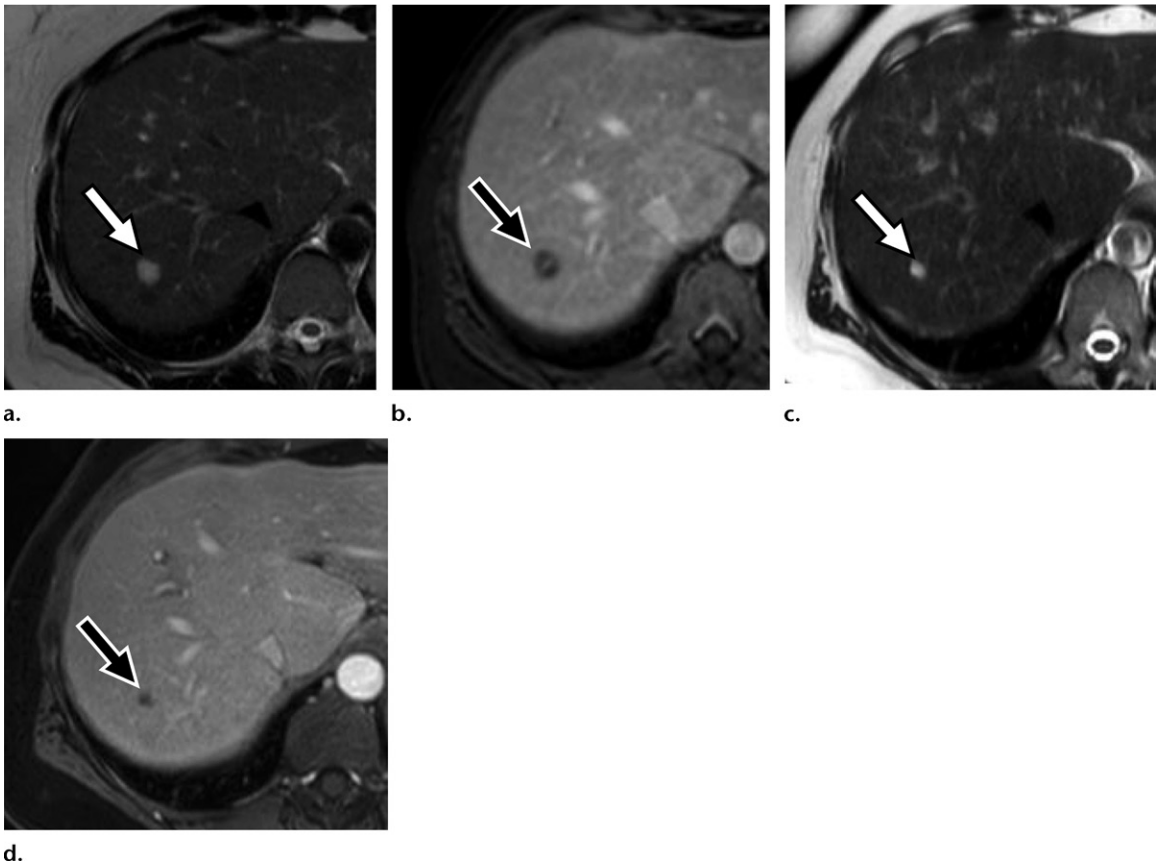

Figure 20. Size reduction of an involuting hemangioma in a 57-year-old woman with cirrhosis due to hepatitis C. **(a)** Baseline axial T2-weighted fat-saturated image shows a mass with marked hyperintensity measuring 11 mm (arrow). **(b)** Axial T1-weighted fat-saturated image in the PVP shows a hypoenhancing mass (arrow). **(c, d)** Corresponding images 8 years later show size reduction of the mass (arrow), which now measures 6 mm. Size reduction favors benignity.

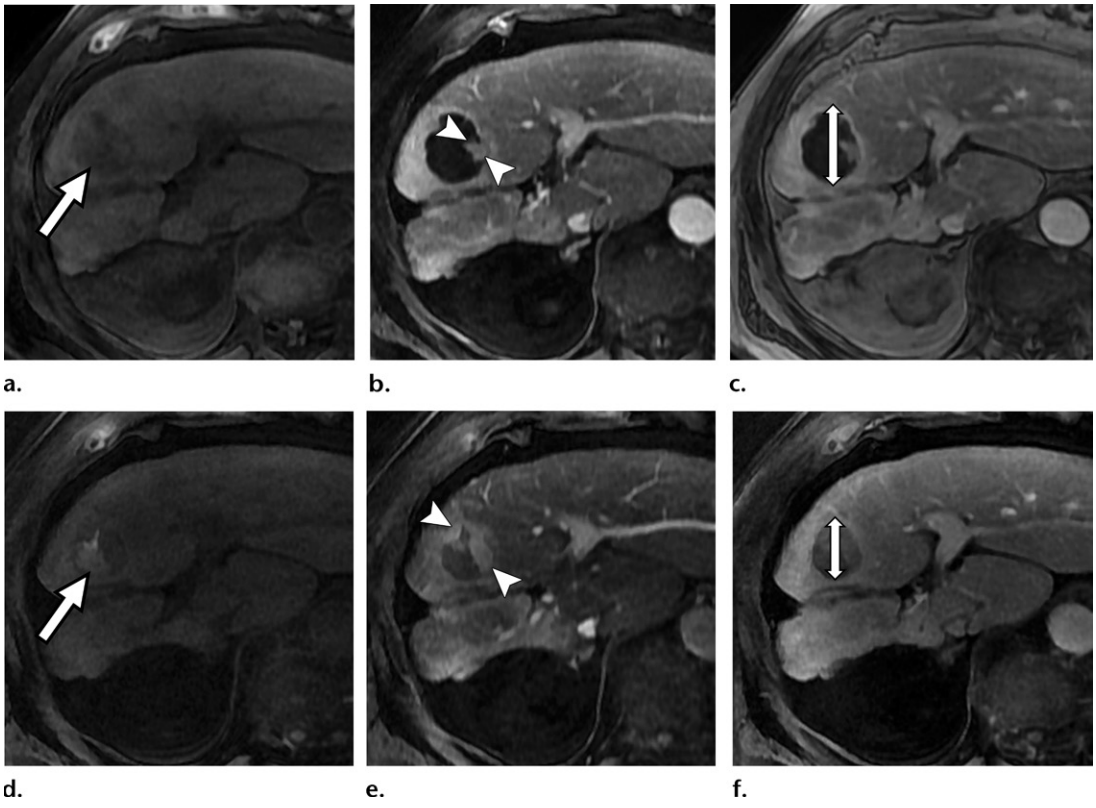

Figure 21. Pitfall of size reduction in a hemorrhagic HCC that shrank owing to resorption of blood products (ie, not owing to benignity). **(a–c)** Baseline axial T1-weighted fat-saturated images before contrast material administra- tion **(a)** and in the late arterial **(b)** and portal venous **(c)** phases show a large hemorrhagic spontaneously hyperin- tense mass (arrow in **a**) with solid enhancing portions (arrowheads in **b**) within a larger mass (double-headed arrow in **c**). **(d–f)** Corresponding images obtained later show blood clot formation (arrow in **d**) and growth of enhancing nodules (arrowheads in **e**) despite overall size reduction of the mass (double-headed arrow in **f**). Size reduction due to resorption of blood products is a pitfall and does not constitute a feature favoring benignity.

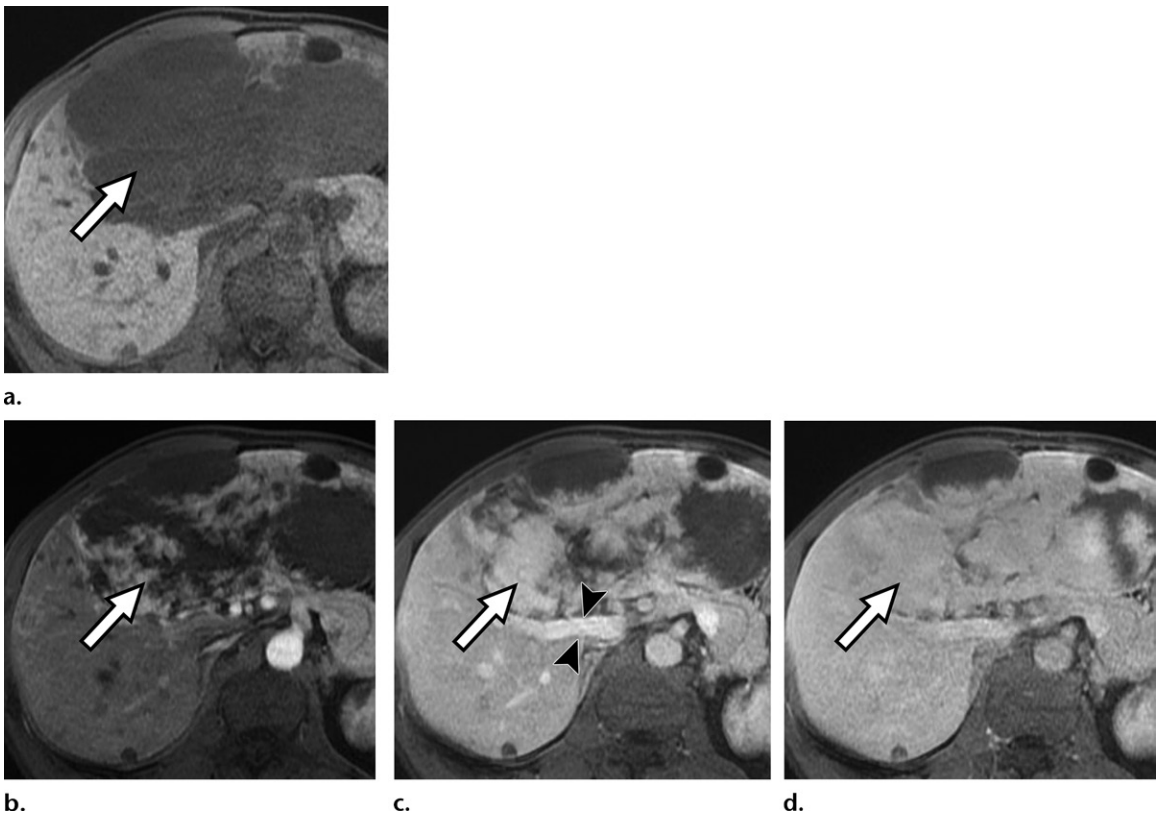

Figure 22. Hemangioma that parallels blood pool enhancement in a 45-year- old man with chronic hepatitis B infection. Axial T1-weighted fat-saturated im- ages before contrast material administration **(a)** and in the late arterial **(b)**, por- tal venous **(c)**, and delayed **(d)** phases show a large mass (arrow) with areas of progressive flame-shaped and nodular enhancement that parallels blood pool enhancement. Arrowheads in **c** = right portal vein.

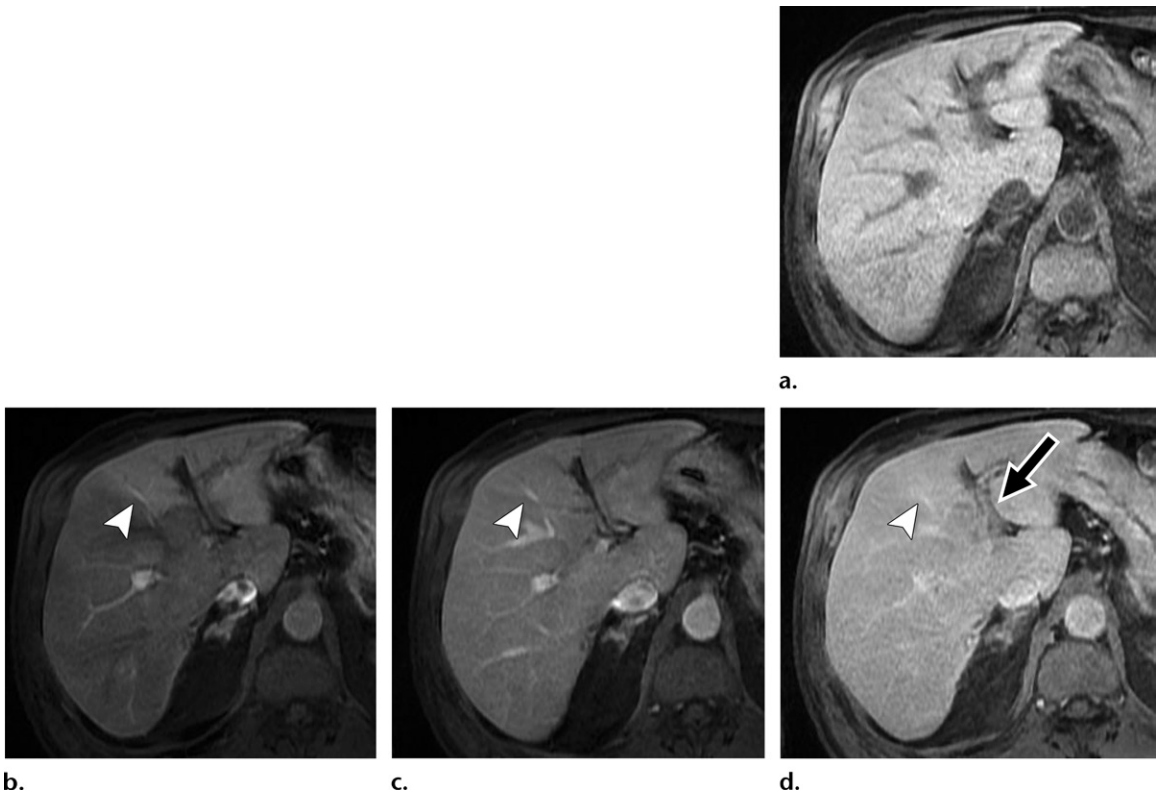

Figure 23. Undistorted vessels in a 64-year-old woman with a bland left portal vein thrombus. Axial T1-weighted fat-saturated images before contrast material administration **(a)** and in the late arterial **(b)**, portal venous **(c)**, and delayed **(d)** phases show an undistorted vessel (arrow in **d**) at the junction of segments IVa and IVb in an area of perfusion alteration visible in the arterial phase (arrowhead in **b–d**) and caused by left portal vein thrombosis. Undis- torted vessels favor benignity.

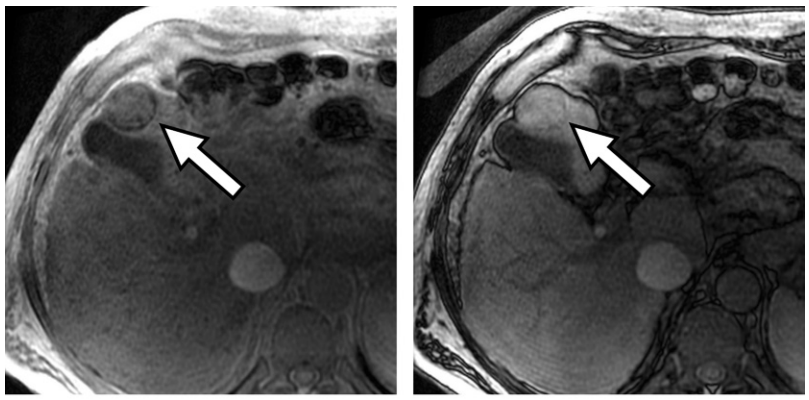

Figure 24. Pitfall of more iron in a mass (HCC) than in the liver in a 50-year-old man with alcoholic cirrhosis. Axial in-phase (TE = 4.6 msec) **(a)** and out-of-phase (TE = 2.3 msec) **(b)** T1-weighted images show iron in a solid mass (arrow) with signal drop observed on the in-phase image, which was obtained with a longer TE. The lesion was categorized LR-5. More iron in a mass than in the liver owing to resorption of blood products is a pitfall and does not constitute a feature favoring benignity.

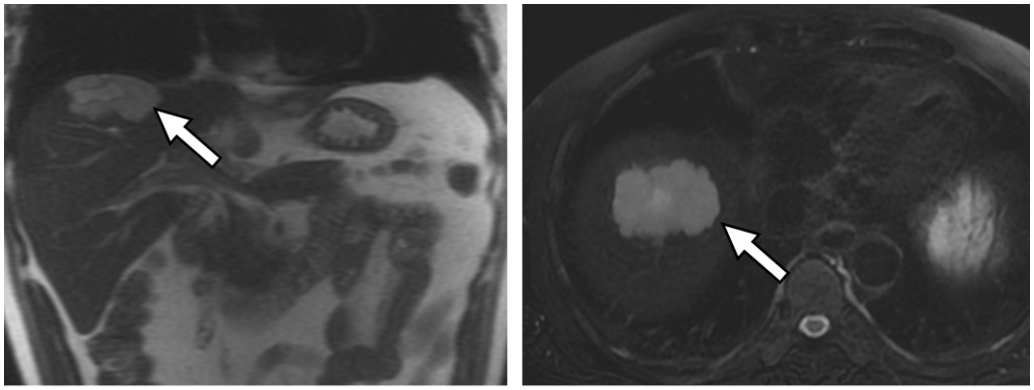

a. b.

Figure 25. Marked T2 hyperintensity of a hemangioma in a 73-year-old man undergoing surveillance for chronic hepatitis B infection. Coronal **(a)** and axial **(b)** T2-weighted fat-saturated images show marked T2 hy- perintensity of a mass (arrow). This imaging feature is diagnostic of hemangioma.

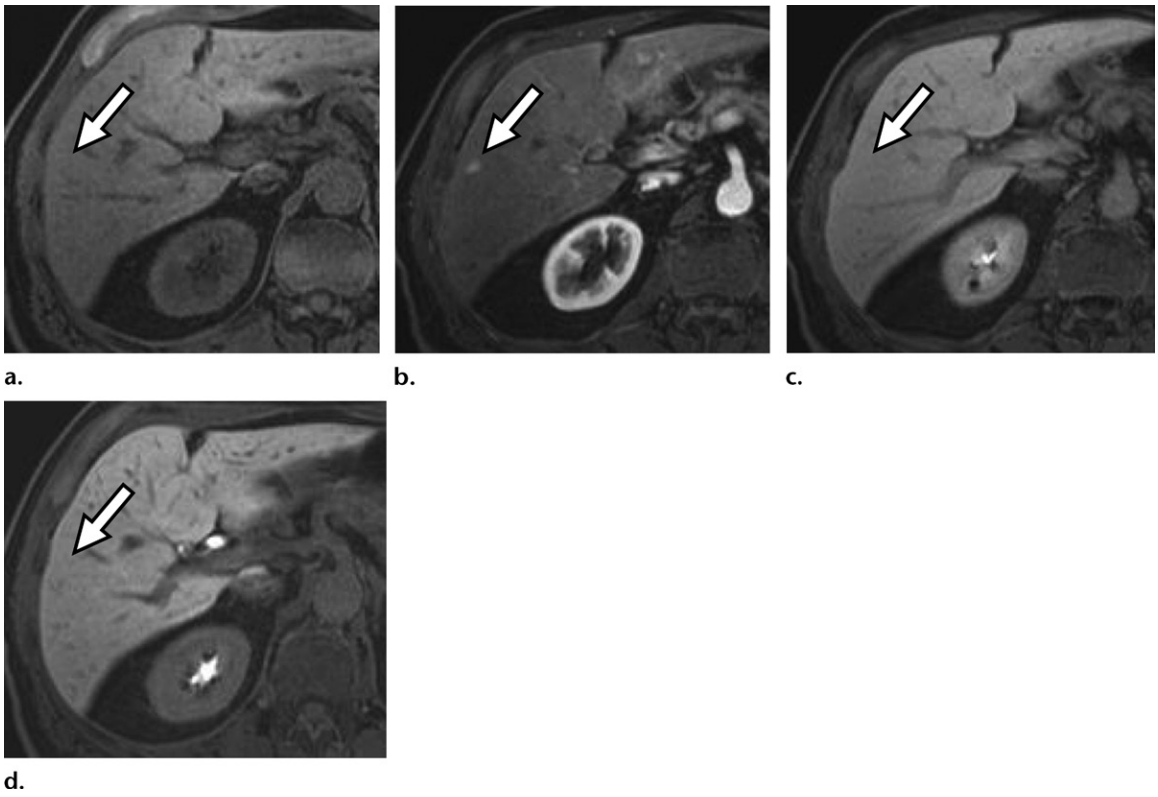

Figure 26. HBP isointensity of a perfusion anomaly in a 67-year-old man. Axial T1-weighted fat-saturated images before contrast material administration **(a)** and in the late arterial **(b)**, transitional **(c)**, and hepatobiliary **(d)** phases show APHE (arrow) with HBP isointensity. HBP isointensity favors benignity.

Figure 27. Effect of ancillary features on LI-RADS categorization of a 25-mm mass in a 50-year-old man. (a–d) Axial T1- weighted fat-saturated images before contrast material administration (a) and in the late arterial (b), portal venous (c), and delayed (d) phases show lack of APHE, washout appearance, or capsule appearance (arrow). According to the diagnostic algo- rithm and table, this observation should be categorized LR-3. (e, f) Axial in-phase (e) and out-of-phase (f) T1-weighted images show signal drop (arrowhead) indicative of intralesion fat. (g, h) Axial diffusion-weighted image (b = 800 sec/mm2) (g) and ADC map (h) show respective hyperintensity (* in g) and hypointensity (* in h) indicative of restricted diffusion. The intrale- sion fat and restricted diffusion led to a category upgrade to LR-4. Pathologic analysis after hepatectomy demonstrated HCC.

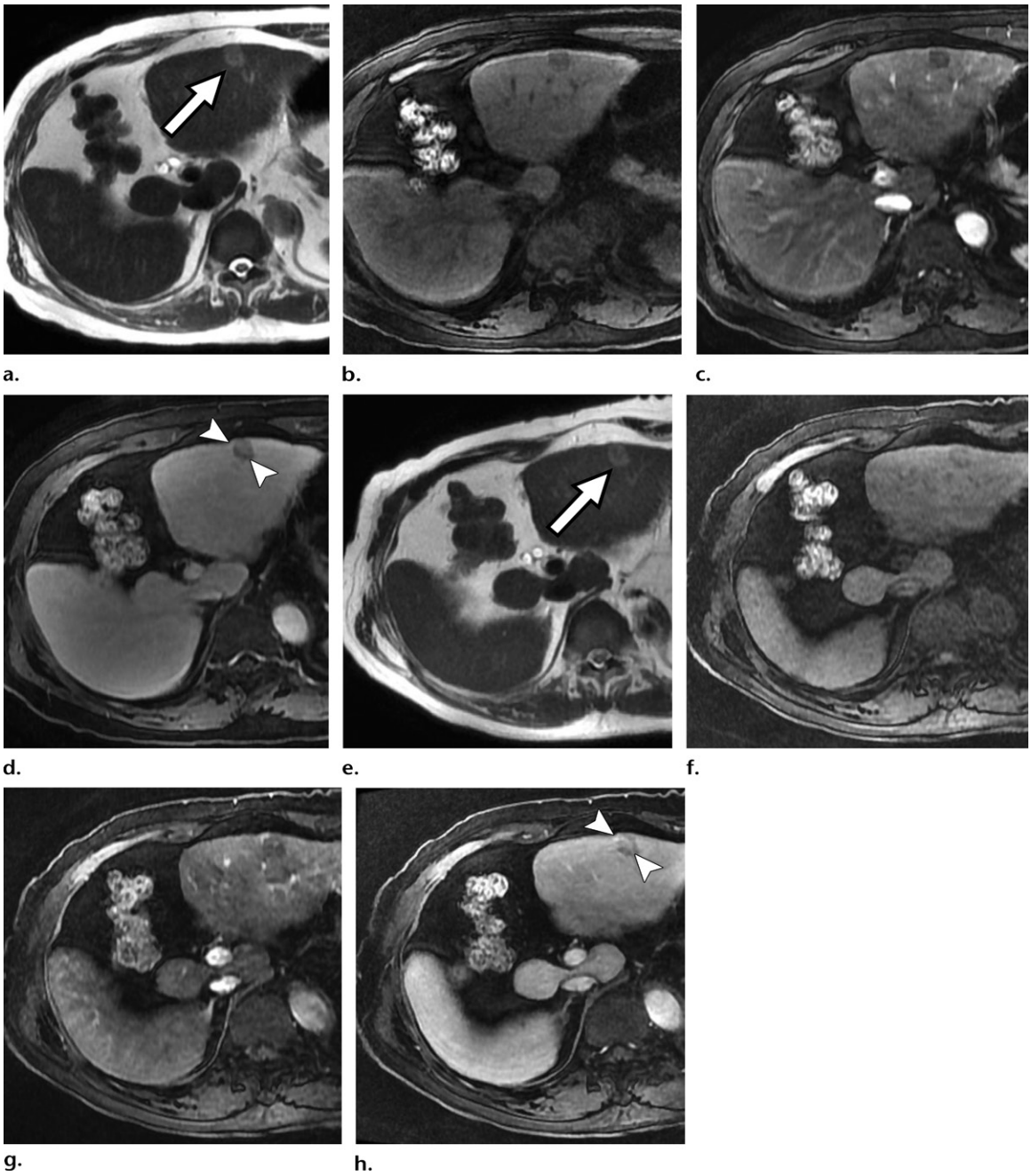

Figure 28. Effect of ancillary features on LI-RADS categorization of a 16-mm mass in a 47-year-old man. **(a–d)** Baseline ax- ial T2-weighted fat-saturated image **(a)** and T1-weighted fat-saturated images before contrast material administration **(b)** and in the late arterial **(c)** and portal venous **(d)** phases show the mass (arrow in **a**, arrowheads in **d**). **(e–h)** Corresponding follow-up images 4 years later show the mass (arrow in **e**, arrowheads in **h**). According to the diagnostic algorithm and table, the observation would be categorized LR-3 because of its size smaller than 20 mm and absence of APHE. Although the observation shows mild-moderate T2 hyperintensity (arrow in **a** and **e**), an ancillary feature favoring malignancy, it also shows stability in size for more than 2 years (arrowheads in **d** and **h**), an ancillary feature favoring benignity. Because of conflicting ancillary features (ie, one or more favoring malignancy and one or more favoring benignity), the category remained unchanged.

Table 1: Ancillary Features in LI-RADS Version 2018

Ancillary features favoring malignancy in general
US visibility as discrete nodule
Subthreshold growth
Corona enhancement
Fat sparing in solid mass
Restricted diffusion
Mild-moderate T2 hyperintensity
Iron sparing in solid mass
Transitional phase hypointensity
Hepatobiliary phase (HBP) hypointensity
Ancillary features favoring HCC in particular
Nonenhancing “capsule”
Mosaic architecture
Nodule-in-nodule architecture
Fat in mass, more than in adjacent liver
Blood products in mass
Ancillary features favoring benignity
Size stability for ≥2 y
Size reduction
Parallels blood pool enhancement
Undistorted vessels
Iron in mass, more than in liver

Table 2: Ancillary Features Favoring Malignancy in General

Feature	Definition	ECA MRI*	HBA MRI†
US visibility as discrete nodule	Unenhanced US visibility as discrete nodule or mass corresponding to MRI-detected observation	+	+
Subthreshold growth	Unequivocal growth of a mass, less than threshold growth	+	+
Corona enhancement	Periobservation enhancement in late arterial phase or early PVP attributable to venous drainage from tumor	+	+
Fat sparing in solid mass	Paucity of fat in solid mass relative to steatotic liver or in inner nodule relative to steatotic outer nodule	+	+
Restricted diffusion	Signal intensity at DWI, not attributable solely to T2WI shine-through, unequivocally higher than in liver and/or ADC unequivocally lower than in liver	+	+
Mild-moderate T2 hyperintensity	Signal intensity at T2WI mildly or moderately higher than in liver and similar to or less than in non–iron-overloaded spleen	+	+
Iron sparing in solid mass	Paucity of iron in solid mass relative to iron-overloaded liver or in inner nodule relative to siderotic outer nodule	+	+
Transitional phase hypointensity	Signal intensity in transitional phase unequivocally less, in whole or in part, than in liver	−	+
HBP hypointensity	Signal intensity in HBP unequivocally less, in whole or in part, than in liver	−	+

Note.—ADC = apparent diffusion coefficient, DWI = diffusion-weighted imaging, HBP = hepatobiliary phase, PVP = portal venous phase, T2WI = T2-weighted imaging.

*MRI performed with an extracellular contrast agent (ECA) can be used to characterize most ancillary features favoring malignancy.

†MRI performed with a hepatobiliary contrast agent (HBA) can be used to characterize all ancillary features favoring malignancy.

Table 3: Diagnostic Performance of Ancillary Features Favoring Malignancy in General at MRI

Ancillary Feature*	References	No. of HCCs (No. of Nodules)	Sensitivity (%)	Specificity (%)	PPV (%)	NPV (%)
Restricted diffusion	Kwon et al 2015 (22)	222 (283)	87	87	85	94
	Hwang et al 2015 (23)	25 (56)	92	84	…	…
	Xu et al 2010 (24)	40 (59)	98	…	…	…
	Inchingolo et al 2015 (25)	29 (53)	97	71	80	94
	Granata et al 2017 (26)	127 (173)	84	100	100	55
	Le Moigne et al 2012 (27)	66 (82)	88	75	…	…
Mild-moderate T2 hyperintensity	Hecht et al 2006 (28)	19 (57)	68	63	…	…
	Hwang et al 2015 (23)	25 (56)	76	87	…	…
	Kim et al 2011 (29)	108 (141)	91	79	…	…
	Granata et al 2017 (26)	127 (173)	100	55	…	…
	Ouedraogo et al 2011 (30)	54 (61)	78	73	…	…
Transitional phase hypointensity	Joo et al 2015 (31)	128 (152)	83–91	33–58	88–91	39–42
HBP hypointensity	Di Martino et al 2016 (32)	71 (118)	75–83	92–96	93–97	71–79
	Ahn et al 2010 (33)	84 (113)	87–92	90–93	…	…
	Golfieri et al 2011 (34)	20 (62)	99	95	99	98
	Sano et al 2011 (35)	96 (108)	94–97	94–96	90–94	97–98
	Haradome et al 2011 (36)	60 (86)	87	90–92	…	…
	Orlacchio et al 2016 (37)	37 (46)	95	90	…	…
	Lee et al 2011 (38)	46 (70)	85	42	…	…
	Sun et al 2010 (39)	44 (97)	93–96	96	95–96	94–96
	Joo et al 2015 (31)	292 (387)	94	48	85	72

Note.—HBP = hepatobiliary phase, NPV = negative predictive value, PPV = positive predictive value.
*Estimates of diagnostic performance are not available for the following ancillary features: US visibility as discrete nodule, subthreshold growth, corona enhancement, fat sparing in solid mass, and iron sparing in solid mass.

Table 4: Ancillary Features Favoring HCC in Particular

Feature	Definition	ECA MRI*	HBA MRI†
Nonenhancing "capsule"	Capsule appearance not detected as enhancing rim	+	+
Mosaic architecture	Presence of randomly distributed internal nodules or compartments, usually with different imaging features	+	+
Nodule-in-nodule architecture	Presence of smaller inner nodule within and having different imaging features than larger outer nodule	+	+
Fat in mass, more than in adjacent liver	Excess fat within mass, in whole or in part, relative to background liver	+	+
Blood products in mass	Intralesion or perilesion hemorrhage in absence of biopsy, trauma, or intervention	+	+

*MRI performed with an extracellular contrast agent (ECA) can be used to characterize all ancillary features favoring HCC.
†MRI performed with a hepatobiliary contrast agent (HBA) can be used to characterize all ancillary features favoring HCC.

Table 5: Ancillary Features Favoring Benignity

Feature	Definition	ECA MRI*	HBA MRI†
Size stability for ≥2 y	No significant change in observation size measured at examinations ≥2 y apart in absence of treatment	+	+
Size reduction	Unequivocal spontaneous decrease in size over time, not attributable to artifact, measurement error, technique differences, or resorption of blood products	+	+
Parallels blood pool enhancement	Temporal pattern in which enhancement eventually reaches and then matches that of blood pool	+	+
Undistorted vessels	Vessels traversing observation without displacement, deformation, or other alteration	+	+
Iron in mass, more than in liver	Excess iron in mass relative to that in background liver	+	+
Marked T2 hyperintensity	Signal intensity on T2-weighted images markedly higher than in liver and similar to that in bile ducts and other fluid-filled structures	+	+
HBP isointensity	Signal intensity in HBP nearly identical to that in liver	−	+

*MRI performed with an extracellular contrast agent (ECA) can be used to characterize most ancillary features favoring benignity.
†MRI performed with a hepatobiliary contrast agent (HBA) can be used to characterize all ancillary features favoring benignity.

Table 6: Diagnostic Performance of Ancillary Features Favoring Benignity at MRI

Ancillary Feature*	References	No. of Benign Entities (No. of Nodules)	Sensitivity (%)	Specificity (%)	PPV (%)	NPV (%)
Parallels blood pool enhancement	Whitney et al 1993 (116)	12 (47)	84	100	…	…
Marked T2 hyperintensity	Whitney et al 1993 (116)	12 (47)	80	100	…	…
	Motosugi et al 2011 (117)	47 (105)	75–91	89–100	…	…
HBP isointensity	Sun et al 2010 (39)	53 (97)	91–94	93	94	89–93

Note.—NPV = negative predictive value, PPV = positive predictive value.
*Estimates of diagnostic performance are not available for the following ancillary features: size stability for ≥2 years, size reduction, undistorted vessels, and iron in mass, more than in liver.